The Effect of Deuteration on Receptor-Ligand Binding

by

Anna Lee

B.Sc., The University of British Columbia, 2013

A THESIS SUBMITTED IN PARTIAL FULFILLMENT OF
THE REQUIREMENTS FOR THE DEGREE OF

MASTER OF SCIENCE

in

The Faculty of Graduate and Postdoctoral Studies

(Physics)

THE UNIVERSITY OF BRITISH COLUMBIA

(Vancouver)

April 2017

Abstract

In this thesis, we use a particle coupled to a phonon bath to accurately model biological and chemical reactions. The path decomposition expansion (PDX) formalism is used to determine the tunneling dynamics of the particle. By decomposing the potential energy landscape into the classically allowed and classically forbidden regions, we can calculate the path integrals associated with each region and connect them to evaluate the full Green's function.

We will also discuss how deuteration of ligand molecules may affect enzyme-substrate binding in GPCR systems. It has been theorized that binding may be dependent on a molecular vibrational component. We investigate this in the β-adrenergic receptor system using the deuterated and non-deuterated forms of the ligand epinephrine. The measurement for successful binding is determined by the amounts of second messenger cyclic-AMP produced. However, our results proved inconclusive and a discussion of possible problems as well as recommendations is included.

Preface

This thesis is original and unpublished work by the author, A. Lee. All of the work presented in Chapter 3 was conducted in Dr. U. Kumar's Laboratory at the University of British Columbia, Point Grey campus. I was responsible for performing biological assays and the analysis of all research data.

The experimental design was conceived by Dr. B. Finlay, Dr. U. Kumar and Dr. R. Somvanshi (University of British Columbia, Vancouver, Canada). All cells used in this experiment were also provided by Dr. U. Kumar.

Table of Contents

List of Figures

Acknowledgements

First, I would like to thank my thesis supervisor Dr. Philip Stamp for his guidance and support on this project. His knowledge proved invaluable during the course of this thesis and I am grateful for his contributions, patience and enthusiasm.

Aside from my supervisor, I would like to thank Dr. Mona Berciu and Dr. Steven Plotkin of the Physics Department for their insightful comments and questions. I would like to thank Dr. Brett Finlay, Dr. Ujendra Kumar and Dr. Rishi Somvanshi for their expertise in the biological experiment and for supplying the time and lab space needed for this experiment.

Lastly, I would like to thank my family for their support and encouragement throughout my entire academic career. This accomplishment could not have been achieved without them.

Dedication

To my parents.

Chapter 1

Introduction

Enzymes are essential to a myriad of physiological processes as they catalyze, or accelerate, chemical reactions. Due to their importance in biological systems, enzyme-substrate binding are widely studied and two prominent theories have been proposed as to how these class of proteins recognize and bind specific substrates. These two theories are the lock-and-key model and the induced-fit model. Enzymes contain a region known as the active site where substrates bind and undergo chemical reactions. In the lock-and-key model, the structure of the substrate fits exactly into the enzyme's active site, allowing the enzyme to recognize only certain ligands. In the induced-fit model, the active site does not exactly match the shape of the substrate. The active site has residues or amino acids that may bind to specific sites on the substrate, causing the enzyme to undergo a conformational change. This change allows the enzyme to bind to the substrate. Once the reaction is completed, the enzyme returns to its initial state. In both models, the success of binding is reliant on the enzyme's ability to recognize the shape and structure of the substrate.

Recently, there has been evidence that binding may also be dependent on a molecular vibrational component. Experiments on olfactory mechanisms performed using *Drosophila melanogaster* (fruit flies) indicate that these flies can differentiate between odourant (smell) molecules whose hydrogens have been replaced with deuterium, and those that have not. Even though the deuterated and non-deuterated molecules have identical structures, flies could be trained to discriminate between them. Further experiments also indicated that molecules without comparable structures but similar vibrational spectra smelled similar to *D. melanogaster* [14]. As olfaction involves a G protein-coupled receptor (GPCR) system, it raises questions as to whether other GPCR systems may also bind substrates or ligands using a molecular vibration-sensing mechanism.

Theories have been developed to explain how changes in molecular vibrational modes can alter receptor-substrate binding. One such theory involves inelastic electron tunneling from a donor site to an acceptor site, a mechanism that is facilitated by the odourant molecule. In this thesis we will study a different model, using a path decomposition approach to determine the tunneling amplitudes for a multidimensional N-well problem that involves electron-phonon coupling.

Experimental results on another GPCR system, the beta-adrenergic system, will also be presented. The effect of deuterated and non-deuterated epinephrine on HEK 293 (human embryonic kidney) cells expressing β_1 adrenergic receptors (β_1AR) and β_2 adrenergic

receptors (β_2AR) will be discussed. This thesis will present evidence on whether differences in the vibrational modes of epinephrine will affect the binding of the ligand to the receptor.

1.1 G Protein and GPCRs

G protein-coupled receptors (GPCRs) form a family of transmembrane proteins that are instrumental in passing signals and sensory stimuli from the outside of the cell to the inside. The activation of the receptor by a ligand, a biomolecule that binds and forms a complex with the receptor, results in a cascade of chemical reactions that leads to the activation of G proteins. Examples of ligands include hormones (signalling molecules), neurotransmitters (chemicals that facilitate nerve impulses), ions and odourants which stimulate sensory receptors (sight and smell respectively). G proteins are a class of regulatory proteins, whose purpose is to form an appropriate response to any incoming stimuli and activate the relevant organs or cells (called effectors) as needed. Essentially, the receptor and G protein form the machinery needed for signal transduction. The GPCR first intercepts the message from the ligand and relays it to the G protein. The G protein then determines the course of action and activates the necessary effectors involved. In this section, more detailed background information on GPCRs and G Proteins and their mechanism of signal transduction will be provided.

About 800 human GPCR sequences have been identified with approximately 460 predicted as being olfactory receptors [15]. As they have an important role in mediating physiological processes, approximately 30% of pharmaceutical drugs are developed to target GPCRs, as defective receptors can lead to pathologies such as heart disease or cancer [23]. GPCRs can be identified by their structural configuration of seven transmembrane alpha-helices connected by alternating intracellular and extracellular loops. The carboxy terminus (C-terminal) is on the inside of the cell while the amino terminus (N-terminal) is on the outside (see Fig. 1.1). GPCRs can be divided into 6 classes based on sequence similarities and structural motifs unique to that class. A description of each class is provided below [10, 19]:

- Class A receptors are also known as rhodopsin-like receptors and form the majority of the GPCR superfamily. This class of receptors includes rhodopsin, a photoreceptor that enables vision in low-light conditions. Although this class is considered to be rhodopsin-like, receptors in this class are diverse and can bind a variety of ligands. These can include peptides and other small biomolecules. Class A receptors share sequence similarities in their transmembrane regions which may play a critical role in their binding capabilities.

- Class B receptors are known as secretin-like receptors as they contain receptors for the peptide hormone secretin. Secretin regulates water balance and intestinal and stomach

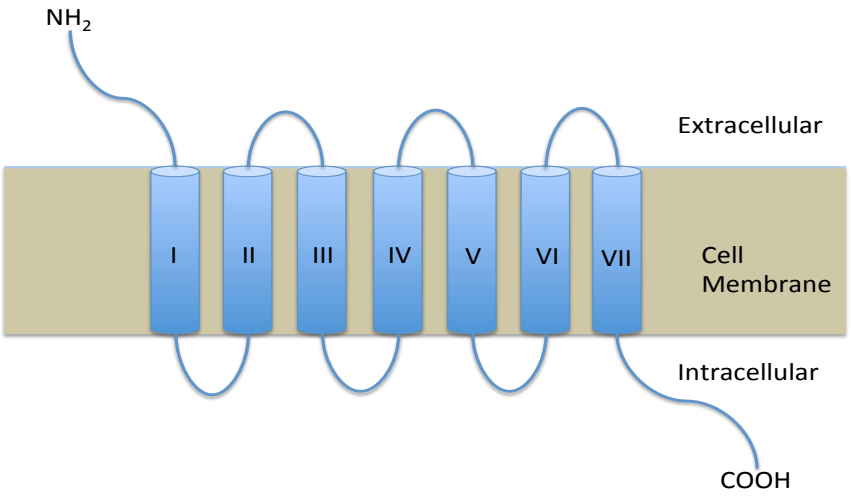

Figure 1.1: All G protein-coupled receptors are characterized by their seven transmembrane alpha helices. These helices are connected by extracellular and intracellular loops. The N-terminal (NH_2) of the receptor is located on the extracellular side of the cell while the C-terminal (COOH) is located on the intracellular side. The above figure depicts the common structural similarities in a GPCR although differences may occur between different classes of receptors.

secretions. About 20 different receptors in this class interact with various neuropeptides and hormones with the N-terminus involved in binding. The N-terminus is very long and contains a network of disulphide bridges. These bridges are strong bonds formed between two cysteine amino acid residues.

- Class C receptors are identified as metabotropic glutamate receptors which are primarily involved in central and peripheral nervous system functions. This class of receptors bind to glutamate, an amino acid that acts as a neurotransmitter. As it is metabotropic, these receptors activate effectors indirectly through secondary messenger molecules. The N-terminus of this class of receptors is also very long (approximately 600 amino acids) and is thought to contain the ligand binding site.

- Class D and E are considered minor families found in fungi.

- Class F consists of the frizzled/smoothened receptor family and is the most recent addition to the classification. Both frizzled and smoothened receptors play a role in cell and embryonic development though they bind to different ligands.

Although the aforementioned receptors and classes all adopt a seven transmembrane

helical configuration, the sequence similarity between each class is very minimal so they can be differentiated structurally [10]. An alternative method of classification, called GRAFS, classifies GPCRs into five groups based on their phylogeny or evolutionary development. In this classification, the families are Glutamate, Rhodopsin, Adhesion, Frizzled/Taste2 and Secretin, which are similar to the previous classification but with the addition of Adhesion and Taste2. Adhesion receptors are involved in proper cell positioning in organs (cell adhesion) and migration, while Taste2 receptors facilitate taste sensation [15].

In order to transduce signals across the cell membrane, GPCRs must interact with G proteins. G proteins are considered molecular switches. In their "off" state, G proteins are inactive. In the "on" state, G proteins can initiate a cascade of chemical reactions in response to a stimulus detected by the GPCR. G proteins consist of three subunits labeled α, β and γ. These subunits are single protein molecules that can assemble with other protein molecules to form one larger complex. The G protein is considered a heterotrimer as the three subunits that form it are not identical. The subunits of the G protein are essential to signal transduction as they relay information from the receptor to various effectors. There are 21 G_α subunits, 6 G_β subunits and 12 G_γ subunits [11]. I will provide a brief overview of the G_α subunit as this subunit provides most of the basic properties of the G protein [41].

All G_α subunits have a region with high binding affinity for guanine nucleotides. Guanine is one of the four main nitrogen-containing biological compounds that serves as a building block for DNA and RNA. Due to a high binding affinity for guanine nucleotides, the G_α subunit can bind to guanosine triphosphate (GTP) and guanosine diphosphate (GDP) compounds, which are simply guanine bases attached to three or two phosphate groups respectively (see Fig. 1.2(a) and 1.2(b)). When the α subunit is bound to GDP, the subunit exists in a complex with the β and γ subunits so the G protein remains in its inactive heterotrimeric state. When the α subunit is bound to GTP, it dissociates from the β and γ subunits and is capable of stimulating effectors. This is considered the "on" state of the protein. These α subunits are enzymes and have weak GTPase activity which allows them to hydrolyze GTP at a slow rate. This allows the α subunits to cleave an inorganic phosphate group from GTP using water and turn it into GDP, thus returning the protein back to its inactive state.

The diverse number of Gα subunits can trigger various signaling pathways. These subunits can be divided into four subfamilies where members of each family will share structural similarities and functionalities [41]. Descriptions of these four groups are provided below and schematically in Fig. 1.3.

- The $G\alpha_{i/0}$ family includes a variety of different subunits ranging from subunits that inhibit adenylyl cyclase ($G\alpha_{i1}$, $G\alpha_{i2}$ and $G\alpha_{i3}$) and α subunits responsible for the signal transduction of taste and vision. Adenylyl cyclase is an enzyme which stimulates the production cyclic AMP (cAMP). Cyclic AMP is an important second messenger

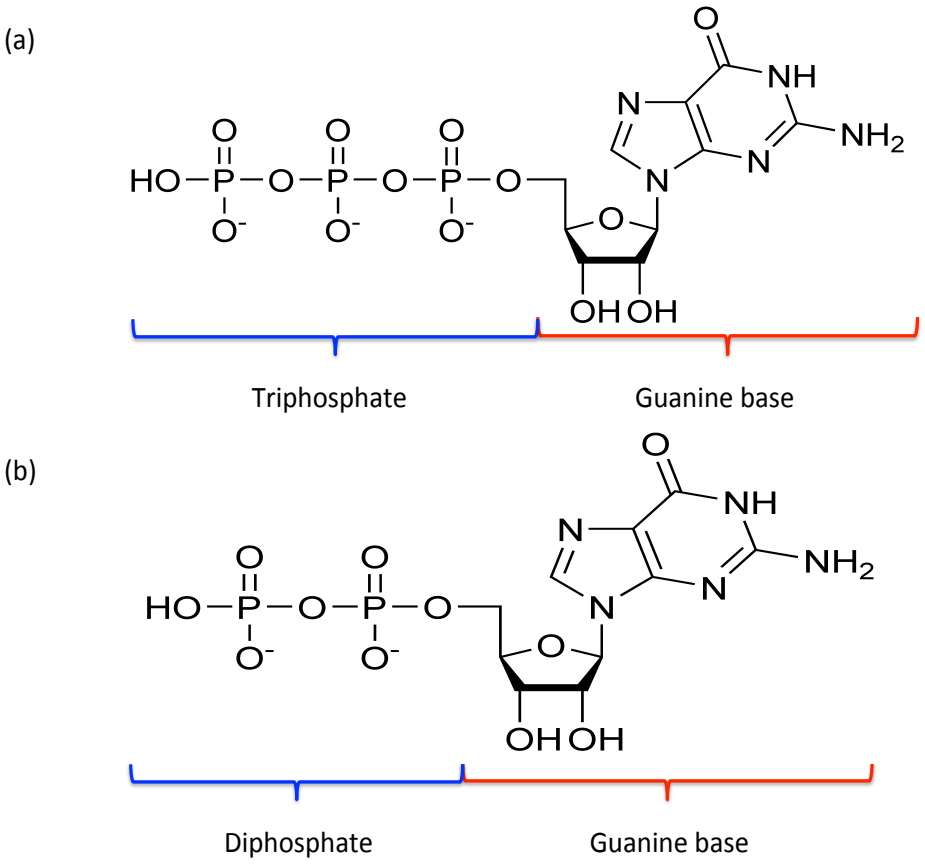

Figure 1.2: (a) The chemical structure of guanosine triphosphate (GTP). GTP consists of a guanine nucleotide and a triphosphate molecule (both indicated in the figure). (b) The chemical structure of guanosine diphosphate, which consists of a guanine nucleotide and a disphosphate molecule. The Gα subunit possesses GTPase activity, allowing it to hydrolyze GTP to GDP by removing an inorganic phosphate group.

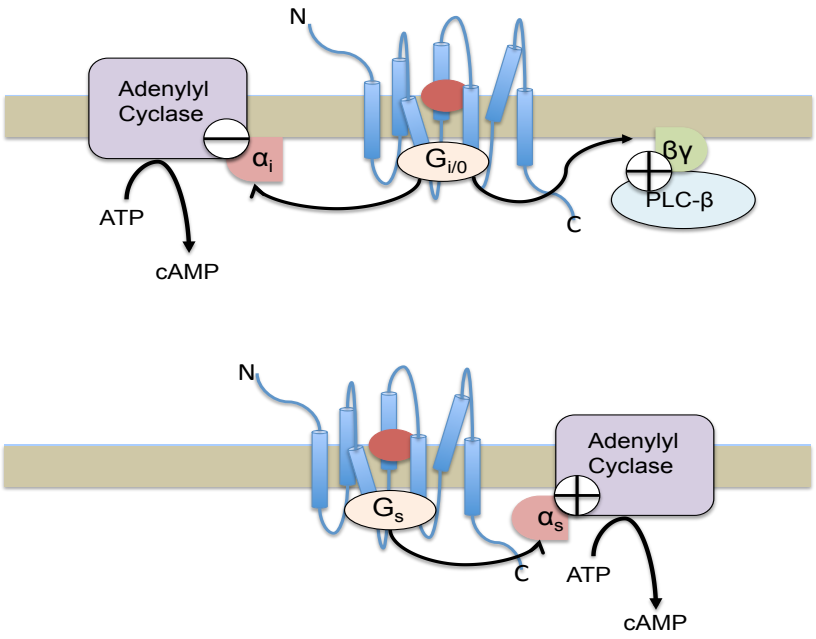

Figure 1.3: A schematic of two of the four subfamilies of Gα subunits. Shown above are the G$\alpha_{i/0}$ and Gα_s subunits. Although the G$\alpha_{12/13}$ and G$\alpha_{q/11}$ subunits are not shown above, the method of activation for the G protein and the dissociation of the α subunits are similar. The ligand binds to its specific GPCR and causes the dissociation of the Gα subunit from the $\beta\gamma$ complex. The Gα subunit and $\beta\gamma$ complex go on to activate their specific effectors and trigger separate signaling pathways. The inhibition or stimulation of an effector is denoted by a minus or plus sign respectively.

that relays signals received from receptors and initiates further intracellular reactions.

- The G$\alpha_{q/11}$ family includes all subunits that are responsible for the activation of phospholipase C-β (PLC-β). Similar to adenylyl cyclase, PLC-β also mediates the production of a second messenger needed for signal transduction.

- The G$\alpha_{12/13}$ subunits stimulate regulatory processes such as transcription (DNA sequences copied into RNA) and cell migration.

- The Gα_s subunits activate adenylyl cyclase to produce more of the second messenger cAMP. The cAMP-dependent pathways regulate signal transduction for olfaction, cell proliferation and differentiation, and maintain physiological conditions at a stable and constant level (homeostasis).

The two subfamilies we will be focusing on in this thesis are the G$\alpha_{i/0}$ and Gα_s subunits. The G$_\alpha$ subunit acts independently during the active state of the G protein while the G$_\beta$

and G_γ subunits form a complex and act as a single unit. The $\beta\gamma$ complex helps stabilize the GDP-bound α subunit and also acts as a membrane anchor. In addition to this, the complex can also stimulate downstream effectors like adenylyl cyclase and phospholipase Cβ1 to Cβ3 [10, 20].

There is a multitude of G proteins that can be made from the various combinations of α, β and γ subunits available. In addition to that, one G protein can couple with various GPCRs and thus stimulate a diverse set of pathways. Despite this, the process of activation can be generalized over all sets of GPCRs, G proteins and ligands. In the inactive state, the receptor is ligand-free and the G protein exists as a heterotrimer with the α subunit bound to GDP. When a ligand binds to the receptor, a conformational change is induced in the receptor and it can now act as a guanine exchange factor (GEF). This allows the receptor to exchange GDP for GTP. The ligand-receptor complex interacts with the G Protein and causes the dissociation of the GDP molecule from the α subunit. With normal cellular concentrations of guanine nucleotides, GTP fills the site immediately causing the G protein to "switch on" and reduces the affinity of the α subunit for the $\beta\gamma$ subunits (Fig. 1.4a). This allows the GTP-α complex to dissociate from the $\beta\gamma$ subunits and each complex can target their downstream effectors (Fig. 1.4b). Eventually the Gα subunit will hydrolyze the GTP molecule bound to it to GDP and an inorganic phosphate (Fig. 1.4c). This terminates the active phase and the GDP-bound α subunit reassociates with the $\beta\gamma$ complex (Fig. 1.4d).

The ligands which trigger the signal transduction mechanism described above can elicit different responses from the GPCR and G protein systems. When the ligand binds to the receptor, the system performs a specific action in response to the ligand. Receptor systems have a constitutive or basal level of activity where the system exhibits a response despite having no ligands bound to the receptor. In the presence of a ligand however, the biological response can be increased or decreased depending on the concentration of ligand present. Bioassays are procedures that are commonly used to measure the biological response as a function of the concentration of ligands present. The resulting data can be used to produce dose-response curves which can determine quantitatively the effect of a ligand on a receptor and whether the ligand is an agonist or antagonist.

Agonists are ligands which can activate receptors to stimulate a higher biological response to the stimuli. They can either be full agonists, which elicit the maximal biological response a receptor is capable of, or a partial agonist which induces a weaker response. Antagonists are ligands which block agonists from binding to the receptor molecule and can dampen receptor activity. Inverse agonists are one type of antagonist that can inhibit activity levels below that of the basal or constitutive levels. Neutral antagonists are incapable of eliciting any stimulation or inhibition from a receptor although they bind to the receptor. Lastly, a biased agonist is a ligand which binds the receptor and signals through G protein-dependent and independent pathways [38]. A schematic of how these different types of agonists and antagonists affect the biological response are provided in Fig. 1.5.

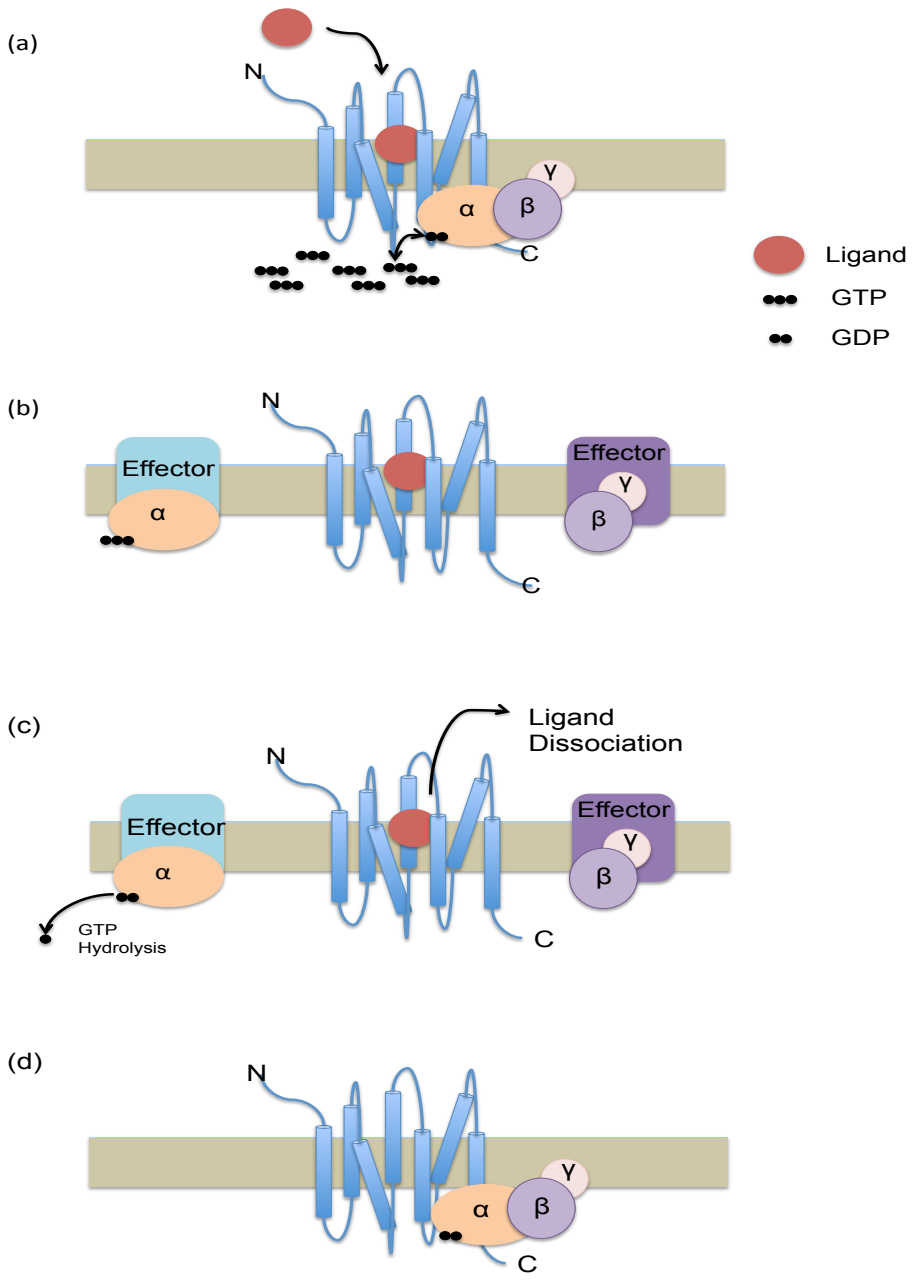

Figure 1.4: The mechanism of signal transduction through a GPCR. (a) The ligand binds to the inactive GPCR, inducing a conformational change in the receptor. The GPCR interacts with the G_α subunit, causing it to exchange GDP for GTP. (b) The α-GTP complex dissociates from the $\beta\gamma$ subunits and each complex targets their downstream effectors. (c) The α subunit eventually hydrolyzes the GTP to GDP. The α subunit reassociates with the $\beta\gamma$ complex and the ligand dissociates from the receptor. (d) The GPCR-G protein returns to their inactive states. A more detailed description is provided in the text.

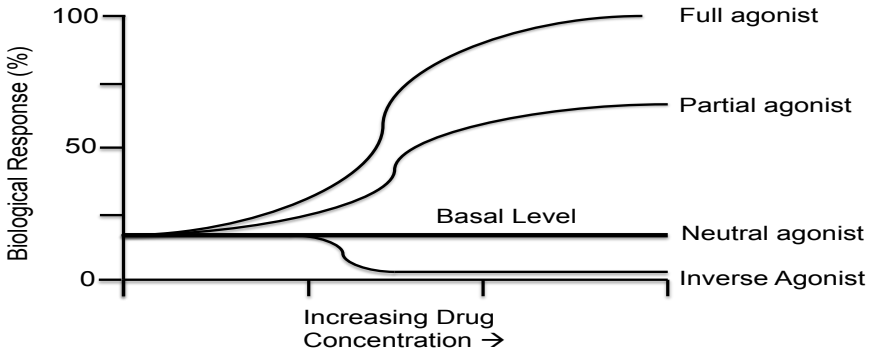

Figure 1.5: The above figure illustrates the biological response of receptors to different types of agonists and antagonists. The basal or constitutive level is the physiological response that occurs in the absence of a bound ligand. A full agonist induces a maximal biological response from the receptor. A partial agonist also stimulates a biological response but induces a weaker level of activity than a full agonist. A neutral agonist neither stimulates or inhibits receptor activity. An inverse agonist can inhibit a biological response and reduce it below the constitutive activity level.

The signal transduction mechanism is well studied in β-adrenergic receptors (β-AR). Adrenergic receptors are targets of catecholamines (benzene molecules with 2 hydroxy groups and an amine side chain). Some well-known catecholamines are epinephrine, norepinephrine and dopamine. There are two main categories of adrenergic receptors, α and β, with various subtypes. This thesis will focus on both β_1 and β_2, although a third subtype exists, called β_3. The β_1ARs are primarily found in the heart and kidneys where they help regulate heart beat and blood pressure. The β_2ARs regulate the function of the smooth muscles of the lung, uterus and blood vessels [5]. Many drugs have been developed that target both these receptors to treat heart disease, hypertension and asthma [36]. The β_2AR was the second GPCR sequenced and cloned after rhodopsin, and was one of the first GPCRs used in radioligand binding assays [27].

Both β_1 and β_2ARs couple to the G_s subunit, although there is some evidence that the coupling of these receptors can switch to G_i depending on agonist concentrations [16, 21, 33, 37]. The binding of epinephrine to the βARs stimulates adenylyl cyclase. Adenylyl cyclase increases the intracellular production of second messenger cAMP, which also leads to the downstream effectors of cAMP (like cAMP-dependent protein kinase, otherwise known as PKA) being activated.

In chapter 3, we will look closely at the β-adrenergic system and how it responds to deuterated and non-deuterated epinephrine. We will attempt to determine whether a molec-

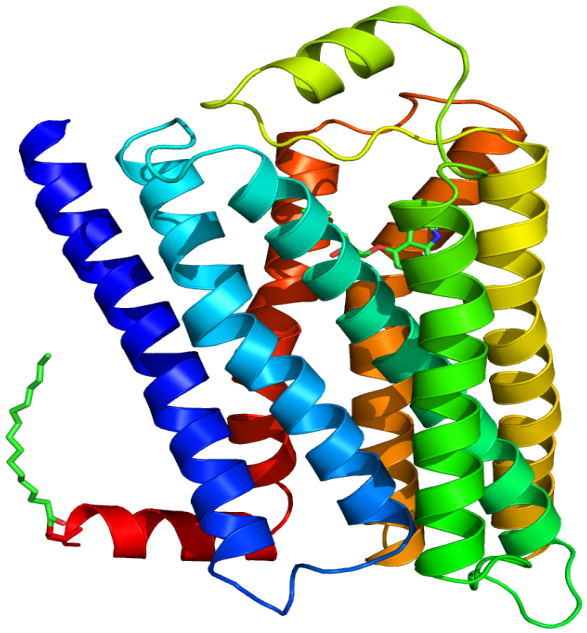

Figure 1.6: The crystal structure of a human engineered β_2 adrenergic receptor bound to the inverse agonist carazolol (denoted by green and red sticks). This figure was produced by S. Jahnichen who has released the figure into the public domain [24].

ular vibration sensing mechanism is used in this GPCR system by performing a cAMP bioassay.

1.2 Inelastic Electron Tunnelling

As mentioned previously, there has been evidence that fruit flies are capable of distinguishing between odourants that are non-deuterated (unaltered) and their deuterated counterparts. As the chemical structures of these molecules are identical, it supports the idea that olfaction may consist of a molecular vibration-sensing component in addition to structural recognition [14]. These experiments have also been performed using humans, although results have been conflicting. Gane et al., 2013 [18], were able to determine that humans could differentiate certain musks, although subjects could not distinguish between the odourants acetophenone and d-8 acetophenone (the deuterated counterpart).

Olfaction mechanisms that rely solely on shape and structure recognition are not capable of describing the phenomenon presented above. As deuterated and non-deuterated molecules essentially possess the same structural properties, notably the same shape and very similar mass, theories that account for a vibrational component must also be discussed. Turin has proposed that receptors act as biological spectrometers capable of detecting inelastic electron tunneling within the system [39].

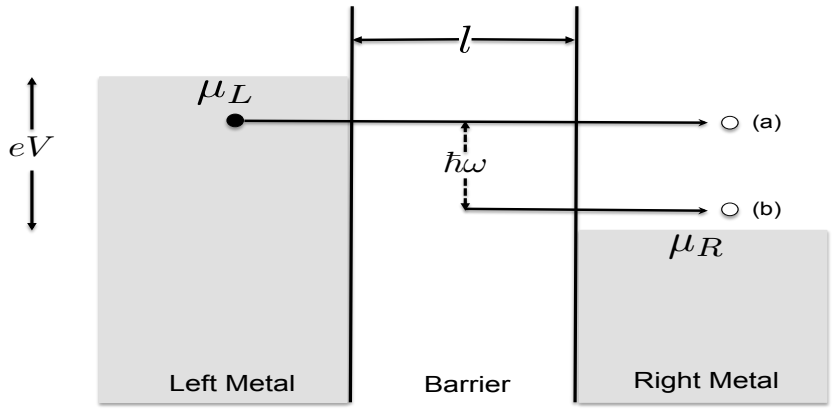

Figure 1.7: A schematic of inelastic electron tunneling. The shaded areas represent the filled electronic states up to the fermi level. (a) Depicts elastic tunneling in which an electron that occupies a state below the Fermi level in the left metal crosses the barrier without any loss of energy and ends in a unoccupied state (white circle) above the Fermi level of the right metal. (b) Illustrates inelastic tunneling where the electron tunnels through to the other side but with an energy loss of $\hbar\omega$. Inelastic tunneling is only possible if $eV \geq \hbar\omega$.

Inelastic electron tunneling spectroscopy (IETS) is a standard experimental technique that is frequently used to study the vibrational modes in a variety of systems. IETS requires a tunnel junction, where a thin insulating barrier is sandwiched between two metal contacts. A voltage is applied between the contacts, which causes the Fermi energy levels of the contacts to become separated by an energy of eV. The thin barrier is usually a metal oxide layer with molecules adsorbed onto it. IETS can be used to study these tunnel junctions and provide information about the vibrational modes of the molecular adsorbates.

Tunneling between the contacts can occur in two ways, through either an elastic or inelastic process (see Fig. 1.7). At $T = 0$, the states in each metal contact are filled up to the Fermi energy and are empty above it. The occupied states on the left contact overlap with the unoccupied states on the right contact. By the exclusion principle, only transitions that start from an occupied state and end at an unoccupied state can occur; therefore, the transitions are determined by the potential difference, V. In an elastic tunneling process, an electron starts from an occupied state on the left contact, tunnels through the barrier and ends in an unoccupied state at the right contact without any loss of energy. The tunneling current produced from this process can be determined by integrating over the probabilities that a particle starts out in an occupied state, ends in an unoccupied state and that it has the ability to penetrate the barrier. We will state the formula here, but more detail can be

found in [4],

$$I = C \int_{-\infty}^{\infty} dE[f(E) - f(E + eV)] \int_{0}^{E} dE_{\perp} \exp(-2 \int_{0}^{l} K dx), \tag{1.1}$$

$$f(E) = [1 + \exp(E/kT)]^{-1}, \tag{1.2}$$

$$K = \frac{2m}{\hbar^2} \sqrt{U(x) - (E - E_{\perp})}, \tag{1.3}$$

where $U(x)$ is the potential energy, E is the total electron energy and $E_{\perp}$ is the kinetic energy of the electron that is perpendicular to the barrier and is equivalent to $\hbar^2 k_{\perp}^2 / 2m$.

If one approximates that the voltage dependence of the barrier is negligible then the current becomes

$$I = C \int_{-\infty}^{\infty} dE[f(E) - f(E + eV)] = CeV \tag{1.4}$$

such that the elastic tunneling process is ohmic, and that its first derivative is constant.

In the inelastic tunneling process, the electron starts off from an occupied state and also tunnels through the barrier. However, in this process the electron loses a quantum of energy, $\hbar\omega$, to a local vibrational mode of the barrier as it crosses. The electron ends in an unoccupied state on the right contact with an energy $\hbar\omega$ less than the initial state. The inelastic electron tunneling process is thus facilitated by the emission of a phonon [22]. Inelastic electron tunneling will only occur if there is an unoccupied state on the right contact that has an energy exactly $\hbar\omega$ less than the occupied state on the left. This process is only possible if the energy difference between the two Fermi levels fulfills the condition that $eV \geq \hbar\omega$. This process provides an additional pathway for the particle to tunnel across the barrier and thus alters the $I - V$ relationship slightly by causing breaks or kinks when $eV = \hbar\omega$. At $T = 0$, these kinks introduce discontinuities in the first derivative, $\partial I / \partial V$, which are then represented as delta functions in the second derivative. Figures 1.8 to 1.10 illustrate the changes in the I-V relationship when inelastic electron tunneling is introduced. If the system being studied has many modes, each of these modes will contribute a delta function in the second derivative at the associated potential difference. Therefore, one could determine the vibrational spectrum by studying the second derivative of the current with respect to the potential.

Turin theorizes that olfactory receptors function as biological spectrometers. The receptor is analogous to the two metal contacts while the odourant molecule is the substance within the gap being studied. As electrons travel from the left contact (donour site) to the right contact (acceptor site), they must pass through the odourant molecule and lose energy to the odourant's local modes. In this fashion, the receptor is capable of distinguishing the odourant from other molecules based on its vibrational spectrum. Turin notes that olfactory receptors fulfill certain requirements needed for electron transfer and inelastic electron tunneling to work in this system. The receptors have conserved binding sites present for

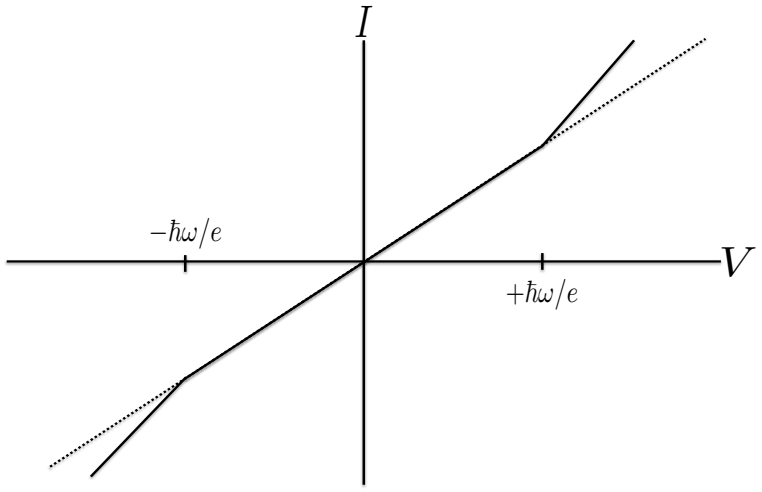

Figure 1.8: A graph of the current against the potential in a tunnel junction at $T = 0$ and when $eV = \hbar\omega$. The elastic tunneling process is linearly proportional to V. The presence of inelastic electron tunneling causes the gradient to skew at $V = \pm\hbar\omega/e$.

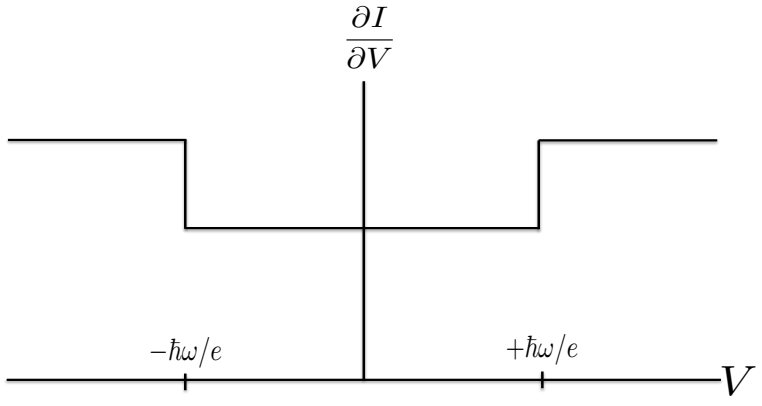

Figure 1.9: A graph of the first derivative of the current against the potential at $T = 0$ and when $eV = \hbar\omega$. Inelastic electron tunneling causes the first derivative to have step-like discontinuities at $V = \pm\hbar\omega$.

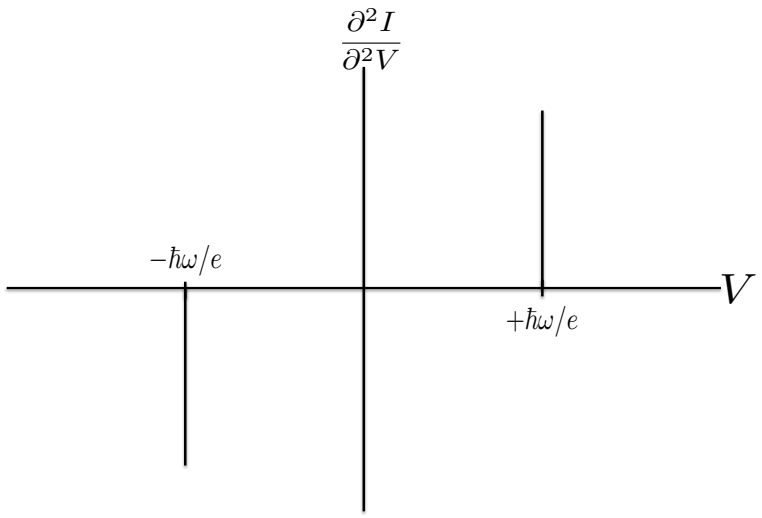

Figure 1.10: A graph of the second derivative of the current against the potential at $T = 0$ and when $eV = \hbar\omega$. The values of V where the delta functions occur can be used to calculate the vibrational spectrum of the molecule in the tunnel junction.

soluble electron carriers and also binding sites for metal cofactors [39]. Metal cofactors (metal ions) are often required for electron-transfer enzymes to function correctly. These characteristics help facilitate electron tunneling within the receptors.

Calculations have also been done to determine whether IETS is a plausible mechanism in olfaction. While these studies determined that IETS could be possible in this system, many assumptions were made regarding the properties of the receptor [3, 40]. It is doubtful that such a model could reliably describe the system and mechanism of olfaction. Furthermore, receptors are complex biomolecules and although they may possess certain properties needed for inelastic electron tunneling, the presence of these is not enough evidence that receptors act as biological spectrometers. A more realistic model is needed to determine how such a system works.

Chapter 2

Tunneling Dynamics of a Particle Coupled to a Phonon Bath

In the previous chapter, we mentioned that there is currently a lack of a realistic model that adequately describes biological and chemical reactions. Here, we will attempt to construct such a model by using a path integral formulation that includes both diagonal and non-diagonal couplings. We will do this by combining the work done by Auerbach and Kivelson, and Caldeira and Leggett.

In section 2.1, we will first discuss the path decomposition expansion (PDX) developed by Auerbach and Kivelson, which uses a connection formula to determine the dynamics of a particle subject to a complicated potential energy landscape. Section 2.2 will then briefly discuss Caldeira and Leggett's work on a particle coupled to a phonon bath, focusing on the effective action. In section 2.3, we will see how the PDX formalism can be applied to a multiwell potential and determine the propagators for a particle traveling in the classically allowed and forbidden regions. In section 2.4, we outline a dual coupling polaron model which provides the diagonal and non-diagonal couplings which are used to determine the spectral functions. We then end this chapter by determining the full Green's function for the particle.

2.1 Path Decomposition Expansion

The path decomposition expansion is a method established by Auerbach and Kivelson to evaluate multidimensional tunneling [2]. There is a variety of instanton techniques that can be used to solve these problems but they tend to have limitations. For instance, these techniques rely heavily on ground-state tunneling paths and so are not suitable for situations where back-scattering is significant or where the initial state is excited [1]. To overcome these limitations, Auerbach and Kivelson developed a multidimensional connection formula which breaks the configuration space into various regions (classically forbidden and allowed) and allows one to solve each region separately. The separation of the regions in configuration space simplifies the calculations and also allows one to tackle problems where the potential energy landscape is very complex. I will first briefly describe the derivation of the path integral formalism and how it can be developed into the path decomposition expansion.

Path integrals provide the transition amplitudes of a particle that moves from a point

x_i at time t_i to a point x_f at time t_f. The propagator, $\hat{G}(t_f - t_i) = exp(-(i/\hbar)\hat{H}(t_f - t_i)$, is the time evolution operator that can be applied to the states of the system to determine the transition amplitude. For example, $G_{x_f,x_i}(t_f - t_i) = \langle x_f | \hat{G}(t_f - t_i) | x_i \rangle$ is the transition amplitude (or 1-particle Green's function) for a particle to move in space-time from (x_i, t_i) to (x_f, t_f).

This form can be extended into the Feynman form for path integrals. The propagator for a many particle system can be written as,

$$G(X_f, X_i; t_f, t_i) = \int_{x(t_i)=X_i}^{x(t_f)=X_f} Dx(t) \exp((i/\hbar)S[x, \dot{x}] \tag{2.1}$$

where $X = (\vec{r}_1, \vec{r}_2, ..., \vec{r}_n)$, and the action is $S[x, \dot{x}] = \int_{t_i}^{t_f} dt L(x, \dot{x}; t)$. The path integration measure, $\int Dx(t)$, is simply the integration of infinitesimal line segments over the entire space. For a 1-dimensional free particle with potential $V(x)$, the Green's function in 1D can be written in terms of infinitesimal line segments as in the following equation:

$$G(x_f, x_i; t_f, t_i) = \lim_{\substack{N\to\infty \\ t\to\infty}} \prod_{j=1}^{N-1} \int dx_j A_N \left\{ \frac{i}{\hbar} dt \sum_{j=1}^{N-1} \left[\frac{m}{2} \left(\frac{x_{j+1} - x_j}{dt} \right)^2 - V(x_j) \right] \right\} \tag{2.2}$$

where $dt = \frac{t_f - t_i}{N}$, $dx_j = x_{j+1} - x_j$ and A_N is the normalization factor. This is the starting point for the PDX formulation.

In the PDX formalism the configuration space can be divided into various regions, usually the classically allowed and forbidden zones. I will begin with an example of where the configuration contains a surface Σ and consists of two regions, inside the surface and outside the surface. The paths originate at a point x_i located inside the surface and end at a point x_f outside the surface. These paths can cross Σ any number of times before exiting the surface one final time at a point x_σ. The point x_σ is the last point where the path touches the surface Σ, and from there the path continues on to the end point x_f (see Fig. 2.1).

As was explained previously, the path integral for a free particle is usually integrated over the entire surface. In this approach however, the paths that cross the point x_σ will not re-enter the interior region of the surface and so the integration limits must reflect this (see Fig. 2.2). The sum over all paths then becomes:

$$G_{N,n} = A_N \int_{-\infty}^{\infty} ... \int_{-\infty}^{\infty} dx_1 dx_2 ... dx_{n-1} \exp\left[-\frac{1}{\hbar} S(0, n-1) \right] \tag{2.3}$$

$$\times \int_{-\infty}^{x_\sigma} dx_n \int_{x_\sigma}^{\infty} ... \int_{x_\sigma}^{\infty} dx_{n+1} dx_{n+2} ... dx_N \exp\left[-\frac{1}{\hbar} S(n-1, N) \right] \tag{2.4}$$

where $S(n_1, n_2) = \sum_{j=n_1}^{n_2} \left[\frac{m(x_{j+1} - x_j)^2}{2dt} + V(x_j) dt \right]$. The above equation is for 1D but can be easily reconfigured for multiple dimensions. The displacements along the surface can

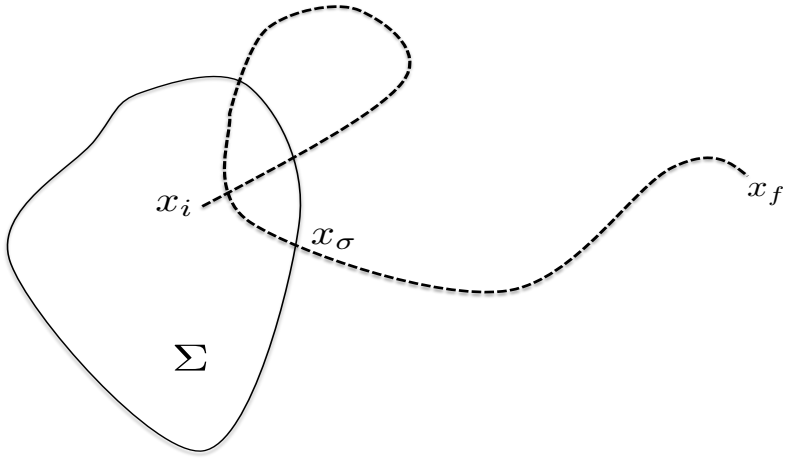

Figure 2.1: The configuration space is split into regions, one which is enclosed by the surface Σ and the other region encompassing all regions which exclude Σ. Paths begin inside Σ at the point x_i and can cross the surface any number of times before finally exiting at the point x_σ and then continuing to the end point at x_f.

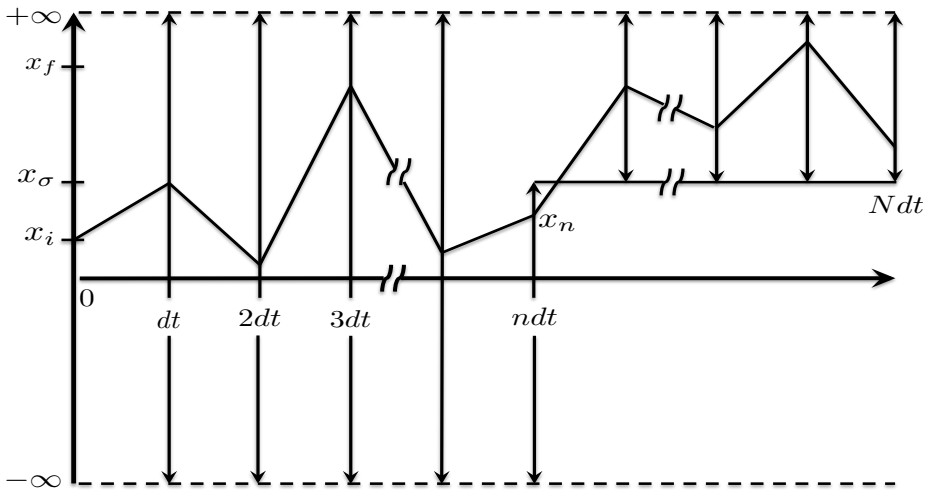

Figure 2.2: A sketch of a possible path the particle can take in moving from the point x_i to the point x_f. The paths are integrated from $-\infty$ to $+\infty$ up until the point x_N as at that point the path must be integrated from $-\infty$ to x_σ. Paths after this are integrated starting from x_σ to $+\infty$ as the paths can no longer traverse the surface Σ.

be parametrized by the components $x_{\sigma,i}$, where $i = 1, 2, ...N$ with $x_{\sigma,1}$ chosen to be along the unit vector $\vec{n}_1$ which is normal to the surface Σ. By changing the integration variables to integrate over the surface, the connection formula becomes:

$$G(x_i, x_f, T) = \int_0^T dt \int_\Sigma d\sigma G(x_i, x, t) \left[\frac{-i\hbar}{2m}\hat{n}_1 \cdot \vec{\nabla}\right] G^{(r)}(x, x_f, T-t)\big|_{x=x_\sigma} \tag{2.5}$$

or in terms of the energy Green's function

$$G(x_i, x_f; E) = \int_\Sigma d\sigma G(x_i, x; E) \left[\frac{\hbar}{2m}\hat{n}_1 \cdot \vec{\nabla}\right] G^{(r)}(x, x_f; E)\big|_{x=x_\sigma} \tag{2.6}$$

where $G(x_2, x_1; E) = \int_0^\infty dt\ \exp(iEt) \int_{x_1}^{x_2} \mathcal{D}X \exp(\frac{i}{\hbar}(S[X] + i\delta t)$ and $\delta \to 0^+$. The Green's function $G^{(r)}$ is called the restricted Green's function and sums over all paths located outside the surface Σ. It can be defined as follows:

$$G^{(r)}(x, x'; E) = \int_0^\infty dt\ \exp(iEt) \int_x^{x'} \mathcal{D}X\ \Theta(X - \Sigma) \exp\left(\frac{i}{\hbar}S[X] + i\delta t\right). \tag{2.7}$$

$G^{(r)}$ contains the same action as G and also satisfies the same differential equation everywhere outside of Σ. It also obeys a Dirichlet boundary condition on the surface which is given by

$$G^{(r)}(x, x'; E)\big|_{x=\Sigma} = 0. \tag{2.8}$$

Eq. 2.6 is the multidimensional connection formula developed by Auerbach and Kivelson. The term $\frac{i\hbar}{2m}\vec{\nabla}_\sigma$ arises from the Jacobian of the change in variables. It can be interpreted as a flux operator and represents the average incoming or outgoing velocities at the point x_σ. Its expression is equivalent to

$$f(x)\vec{\nabla}g(x) = \left[f(x)\partial_x g(x) - g(x)\partial_x f(x)\right]. \tag{2.9}$$

We will express the flux operator as

$$[\Sigma] = \lim_{x,x'\to x_\sigma} \int_\Sigma d\sigma\, |x_\sigma\rangle \langle x| \left[\frac{\hbar}{2m}\hat{n}_1 \cdot \vec{\nabla}\right] |x'\rangle \langle x_\sigma| \tag{2.10}$$

and will use this to simplify the notation for the full Green's function.

The PDX connection formula provided above was only for two regions, however this formula can easily be extended for multiple decomposition surfaces, Σ_i, where $i = 1, ..., N$. We will define the transition matrix t_{ij} as

$$t_{ij} = [\Sigma_i] g_{ij} [\Sigma_j] \tag{2.11}$$

where g_{ij} is the restricted Green's function which starts and ends at points $x_{\sigma,i}$ and $x_{\sigma,j}$, which belongs to surfaces $[\Sigma_i]$ and $[\Sigma_j]$ respectively, but does not enter the interior of any surface. We will first begin with an example of a 2-surface problem which splits the configuration space into 3 regions. If the particle were to begin its path starting from x_1 at Σ_1 and end in the same location, the particle can take a multitude of paths, one where the particle stays within the well, one where the particle travels to Σ_2 and back, and paths where it constantly moves back and forth between the two sites. This is summarized in the following equation:

$$\mathcal{G}_{11} = \langle x_1 | \, g_1 + g_1 t_{12} g_2 t_{21} g_1 + g_1 t_{12} g_2 t_{21} g_1 t_{12} g_2 t_{21} g_1 + ... \, | x_1 \rangle \tag{2.12}$$

where here g_1 is the local Green's function for the site centred at Σ_1. We can see that this is a geometric series and that the full Green's function can also be rewritten as

$$\mathcal{G}_{11} = \langle x_1 | \, [g_1^{-1} - t_{12} g_2 t_{21}]^{-1} \, | x_1 \rangle \, . \tag{2.13}$$

We will now try to generalize the full Green's function for cases where there are more than 2 potentials and where the initial and final points are not identical. We note that for a full Green's function the sum can be expressed as

$$\mathcal{G}_{\alpha\beta} = g_\alpha \delta_{\gamma\beta} + g_\alpha t_{\alpha\beta} g_\beta + g_\alpha t_{\alpha\gamma_1} g_{\gamma_1} t_{\gamma_1\beta} g_\beta + g_\alpha t_{\alpha\gamma_1} g_{\gamma_1} t_{\gamma_1\gamma_2} g_{\gamma_2} t_{\gamma_2\beta} g_\beta + ... \tag{2.14}$$

where α represents the initial site, β the final site, and γ_n (where $n = 1, 2, 3...$) represents the intermediate sites the particle travels to. One can see here that only certain paths are allowed within the full Green's function, as indicated by the indices, and so the summation must be done carefully. We note that the above expression contains the pattern $t + tgt + tgtgt + ...$ which allows us to write two recursion formulas for the full Green's function:

$$T_{\alpha\beta} = t_{\alpha\beta} + t_{\alpha\gamma} \mathcal{G}_{\gamma\delta} t_{\delta\beta}, \tag{2.15}$$

$$\mathcal{G}_{\alpha\beta} = g_\alpha \delta_{\alpha\beta} + g_\alpha T_{\alpha\beta} g_\beta. \tag{2.16}$$

Eq. 2.15 and 2.16 ensure that only allowed paths are included in the full Green's function.

The path decomposition expansion is very useful for multidimensional tunneling problems with complicated potential landscapes. While there is a multitude of instanton techniques available to solve these problems, they tend to focus on the forbidden region and ignore the classical regions. The PDX formalism allows one to decompose a complicated problem into manageable pieces that can be solved separately. This allows one to evaluate both the forbidden and classically allowed regions which can provide more physical insight to the problem.

Using the PDX formalism, we will attempt to realistically model and solve a multiwell

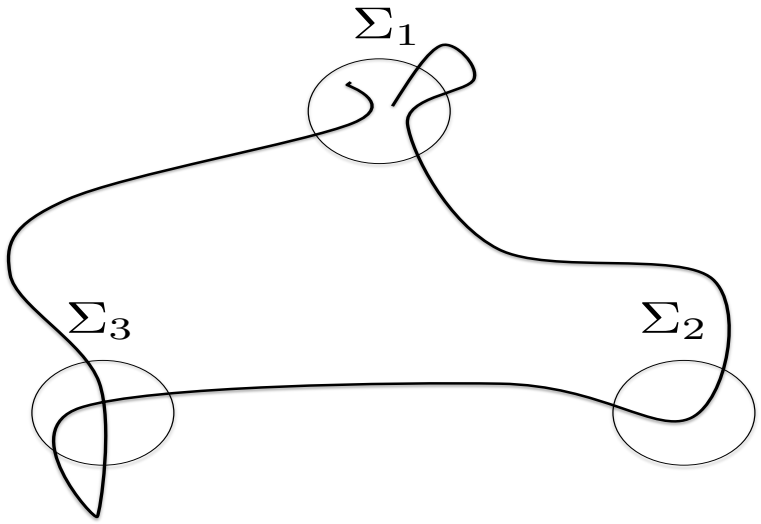

Figure 2.3: A sketch of a possible path taken by a particle which starts and ends at Σ_1. The path runs from Σ_1 to Σ_2 to Σ_3 before finally ending at Σ_1. This is one of many paths that a particle can take starting at Σ_1 and then returning to the same surface.

quantum tunneling problem. We will look at the multiwell problem as done by Auerbach and Kivelson but also include the system's interaction with an environment consisting of phonons. This will ensure that we realistically model what occurs in chemical and biological reactions.

2.2 Quantum Tunneling with Phonon Coupling

In chemical and biological reactions, the interaction between the system and environment may play a significant role in the reaction dynamics. To realistically simulate these interactions, we will include an environment consisting of harmonic oscillators coupled to the particle system. We will introduce one restriction to simplify the calculations: the system is only weakly coupled to each environmental mode, ensuring that each environmental mode is only weakly perturbed. This restriction will lead to a Lagrangian that can be used to represent various dissipative systems [6].

The phonon coupling can be included in the PDX method mentioned in the previous section to determine how phonon modes can mediate the tunneling of a particle through the potential energy landscape. We will approach this problem using the Lagrangian formulation of quantum mechanics and make use of influence functionals, which were defined by Feynman and Vernon (1963) [13]. We will then look at the effective action that results and see how this will fit into the PDX formalism.

A Lagrangian which describes a system interacting with an environment of phonons is:

$$L = \frac{1}{2}M\dot{q}^2 - V(q) + \frac{1}{2}\sum_j (m_j\dot{x}_j^2 - m_j\omega_j^2 x_j^2) - \sum_j F_j(q)x_j - \sum_j F_j^2(q)/2m_j\omega_j^2 \tag{2.17}$$

where the first two terms describe the particle (system) whose displacement is denoted by q, the third term describes the harmonic oscillators (environment) denoted by x_j, the fourth term describes the interaction between the system and environment and the last term is a counter-term which renormalizes the potential. We choose the term $\sum_j F_j(q)x_j$ to be bilinear such that

$$F_j(q) = C_j q. \tag{2.18}$$

All information about the effects of the environment on the system is then incorporated in the spectral density

$$J(\omega) \equiv \frac{\pi}{2}\sum_j \frac{C_j^2}{m_j\omega_j}\delta(\omega - \omega_j). \tag{2.19}$$

With the above general Lagrangian, we can determine the density matrix in equilibrium for the system and environment as

$$\rho(q_i, \{x_{ji}\}; q_f, \{x_{jf}\}; \beta) \equiv \sum_n \psi_n^*(q_i, \{x_{ji}\})\psi_n(q_f, \{x_{jf}\}) \exp(-\beta E_n), \tag{2.20}$$

where q_i and q_f represent the initial and final values for the particle coordinates respectively, x_{ji} and x_{jf} represent the endpoints for the harmonic oscillators and ψ_n represents the combined state of the system and environment. The general Lagrangian for this problem can be split into two parts, one which is dependent on the system only and another which depends on the oscillator coordinates and the bilinear interaction. As we are only interested in the dynamics of the system, the environmental coordinates can be traced over to obtain the following propagator

$$G(q_i, q_f, T) = \int \prod_j dx_{ji} \int_{q(0)=q_i}^{q(T)=q_f} \mathcal{D}q(\tau) \prod_j \int_{x_j(0)=x_{ji}}^{x_j(T)=x_{ji}} \mathcal{D}x_j(\tau) \tag{2.21}$$

$$\times \exp\left(-\int_0^T L(q, \dot{q}; \{x_j, \dot{x}_j\})d\tau/\hbar\right) \tag{2.22}$$

where L is the Lagrangian given in Eq. 2.17 with the bilinear coupling.

We can perform this trace by noting that the environment coordinates x_j and $\dot{x}_j$ are in

either quadratic or linear powers. The integral to be evaluated is

$$Q(\tau) = \int dx_i \int_{x(0)=x_i}^{x(T)=x_f} \mathcal{D}x(\tau) \exp\left\{-\frac{1}{\hbar}\int_0^T \left(\frac{1}{2}m\dot{x}^2 + \frac{1}{2}m\omega^2 x^2 - Cqx\right) d\tau\right\} \tag{2.23}$$

which contains the action for a driven harmonic oscillator. This integral can be solved in various ways. One method that provides the simplest result is detailed in [12]. We refer the reader to [12] for further details and will state the result here:

$$Q(\tau) = \exp\left\{-\frac{1}{4m\omega\hbar}\int_0^T \int_0^T \frac{\cosh\omega(|\tau-\tau'| - \frac{1}{2}T)}{\sinh\frac{1}{2}\omega T} q(\tau)q(\tau')d\tau d\tau'\right\}. \tag{2.24}$$

If we specify that $q(\tau)$ outside of $0 \leq \tau \leq T$ be periodic with period T, then the expression above can be simplified to

$$Q(\tau) = \frac{1}{2}\text{cosech}\frac{\omega T}{2} \exp\left\{\frac{C^2}{4m\omega\hbar}\int_{-\infty}^{\infty} d\tau' \int_0^T d\tau e^{-\omega|\tau-\tau'|} q(\tau)q(\tau')\right\}. \tag{2.25}$$

Now inserting this term into the propagator we find

$$G(q_i, q_f; T) = G_0(T) \int_{q(0)=q_i}^{q(T)=q_f} \mathcal{D}q(\tau) \exp[-S_{\text{sys}}/\hbar] \exp[\Lambda/\hbar] \tag{2.26}$$

where

$$G_0(T) = \prod_j \frac{1}{2}\text{cosech}\frac{\omega_j T}{2}, \tag{2.27}$$

$$S_{\text{sys}}[q(\tau)] = \int_0^T \left(\frac{1}{2}M\dot{q}^2 + V(q)\right) d\tau, \tag{2.28}$$

$$\Lambda[q(\tau)] = \int_0^T \frac{1}{2}M\Delta\omega^2 q^2(\tau)d\tau + \sum_j \left\{\frac{C_j^2}{4m_j\omega_j}\int_{-\infty}^{\infty} d\tau' \int_0^T d\tau e^{-\omega_j|\tau-\tau'|} q(\tau)q(\tau')\right\}. \tag{2.29}$$

The form of $\Lambda[q(\tau)]$ can be simplified by noting that

$$q(\tau)q(\tau') = \frac{1}{2}\{q^2(\tau) + q^2(\tau') - (q(\tau) - q(\tau'))^2\} \tag{2.30}$$

and by inserting this into $\Lambda[q(\tau)]$ we can integrate $q^2(\tau)$and $q^2(\tau')$ over $d\tau$ and $d\tau'$ respectively. Performing this integration results in canceling out the first term in $\Lambda[q(\tau)]$ so that the resulting form is

$$\Lambda[q(\tau)] = -\frac{1}{2}\int_{-\infty}^{\infty} d\tau' \int_0^T d\tau\ \alpha(\tau-\tau')\{q(\tau) - q(\tau')\}^2, \tag{2.31}$$

where

$$\alpha(\tau - \tau') \equiv \sum_j \frac{C_j}{4m_j\omega_j} \exp(-\omega_j|\tau - \tau'|) \tag{2.32}$$

$$\equiv \frac{1}{2\pi}\int_0^\infty J(\omega)\exp(-\omega|\tau - \tau'|)d\omega \geq 0 \tag{2.33}$$

where $J(\omega)$ is the spectral density defined in Eq. 2.19. The propagator for a particle linearly coupled to a bath of harmonic oscillators is expressed as

$$G(q_i, q_f, T) = G_0(T)\int_{q(0)=q_i}^{q(T)=q_f} Dq(\tau)\exp[-S_{\text{eff}}[q(\tau)]/\hbar] \tag{2.34}$$

where the effective action is given by

$$S_{\text{eff}}[q(\tau)] = \int_0^T \left\{\frac{1}{2}M\dot{q}^2 + V(q)\right\}d\tau + \frac{1}{2}\int_{-\infty}^{\infty} d\tau' \int_0^T d\tau\alpha(\tau - \tau')\{q(\tau) - q(\tau')\}^2. \tag{2.35}$$

The above result has been used in various papers to determine the tunneling dynamics of a particle coupled to a phonon bath. In [6] and [29], the authors determine the dynamics by first truncating the high frequency modes of the harmonic oscillators in order to generate a two-state system called the spin-boson system. While we will not describe the details of the truncation in this thesis, we will mention that in this method they introduce an artificial cutoff for the spectral density in order to split the low and high frequency modes of the bath.

Instead of introducing an artificial cutoff, we will determine the effective action for a particle traveling in a phonon bath by adopting a dual coupling polaron model. This method will better determine the dynamics as it includes both diagonal and non-diagonal couplings and does not include an unphysical cutoff.

2.3 Applying the PDX Formalism to a Multiwell Potential

In this section, we will see how the effective action can be used to determine the propagators for regions in the classically allowed and forbidden regions. Only a brief overview will be provided so the reader is encouraged to see [6] and [29] for more detail.

As was mentioned previously, the spectral density incorporates all effects the environment, in this case the phonon bath, has on the system. This includes the effects of both the diagonal and non-diagonal couplings. In the classically allowed regions, the diagonal couplings can be used to determine the spectral density while the forbidden regions are associated with the non-diagonal couplings. By inserting these spectral densities into the propagator, we can determine the propagators for a particle coupled to a phonon bath.

To apply the PDX formalism to a multidimensional well, one must split the configuration

space into various regions. For example, Fig. 2.4 depicts an asymmetrical well in which the ground state energies are separated by an energy $\tilde{\epsilon}$ and the minima are located at $\pm q_0/2$. For such a potential, we can first split the potential into three separate regions. Regions I and III comprise of surfaces which enclose the potential wells while region II encompasses the area between the two wells (e.g. the forbidden region). One can solve the path integral within each region and then simply connect the propagators via the PDX formalism described in the previous section. We will see how one calculates the path integrals within the classically allowed and forbidden regions in the next two subsections.

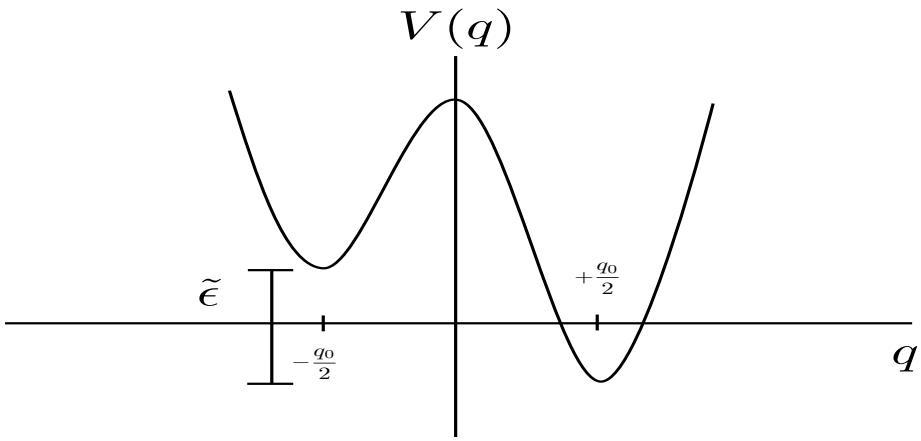

Figure 2.4: Sketch of an asymmetric well with potential minima located at coordinates $\pm q_0/2$.

2.3.1 Path Integral in the Classically Allowed Region

We will begin by determining the path integrals for a particle coupled to bath oscillators within the potential wells. The propagator, as we have seen previously, can be represented as follows

$$G(q_i, q_f; \beta) = \text{const} \exp[-S_{\text{cl}}(q_i, q_f; \beta)] \tag{2.36}$$

where S_{cl} is the action evaluated along the classical path starting at q_i at time zero and ending at q_f at time β. To simplify the expression of the effective action, we will take its

Fourier transform. The Fourier transforms are

$$Q(\omega) = \int_{-\infty}^{\infty} q(\tau) e^{-i\omega\tau}, \tag{2.37}$$

$$q(\tau) = \frac{1}{2\pi} \int_{-\infty}^{\infty} d\omega Q(\omega) e^{i\omega\tau}. \tag{2.38}$$

Inserting these fourier transforms into the effective action, we obtain

$$\begin{aligned} S_{\text{eff}}[Q(\omega)] =& \frac{1}{2\pi} \int_{-\infty}^{\infty} d\omega \int_{-\infty}^{\infty} d\omega' \frac{1}{2} M(-\omega\omega') Q(\omega) Q(\omega') \delta(\omega + \omega') + S_V \\ &+ \frac{1}{2} \int\int\int\int d\tau d\tau' d\omega' d\omega'' \int_0^{\infty} \frac{d\omega}{(2\pi)^3} J(\omega) e^{-\omega|\tau-\tau'|} Q(\omega') (Q(\omega'') e^{i\tau(\omega+\omega')} \\ &\times \left(1 - e^{i\omega'(\tau'-\tau)} - e^{i\omega''(\tau'-\tau)} + e^{i(\omega'+\omega'')(\tau'-\tau)}\right). \end{aligned} \tag{2.39}$$

In the last term, we let $s = \tau' - \tau$ and then integrate over $d\tau$. The last term then takes the form

$$\begin{aligned} &\frac{1}{2} \int\int\int ds d\omega' d\omega'' \int_0^{\infty} \frac{d\omega}{(2\pi)^2} J(\omega) e^{-\omega|-s|} Q(\omega') Q(\omega'') \delta(\omega' + \omega'') \\ &\qquad \times \{1 - e^{i\omega' s} - e^{i\omega'' s} + e^{i(\omega'+\omega'')s}\} \\ &= \frac{1}{2(2\pi)^2} \int\int\int d\omega d\omega' Q(\omega') Q(-\omega') \left\{ 2 \int_{-\infty}^{\infty} ds J(\omega) e^{-\omega|-s|} \right. \\ &\qquad \left. -2 \int_{-\infty}^{\infty} ds J(\omega) e^{\omega|-s|} e^{-i\omega' s} \right\} \\ &= \frac{1}{(2\pi)^2} \int\int d\omega d\omega' Q(\omega') Q(-\omega') J(\omega) \left\{ \int_{-\infty}^{0} e^{\omega s} ds \right. \\ &\qquad \left. + \int_0^{\infty} e^{-\omega s} ds \int_0^{\infty} e^{s(\omega - i\omega')} ds + \int_{-\infty}^{0} e^{is(\omega + i\omega')} ds \right\} \\ &= \frac{1}{2\pi^2} \int\int d\omega d\omega' Q(\omega') Q(-\omega') J(\omega) \left\{ \frac{1}{\omega} - \frac{\omega}{\omega + \omega'^2} \right\} \\ &= \frac{1}{2\pi^2} \int\int d\omega d\omega' Q(\omega') Q(-\omega') J(\omega) \left(\frac{\omega'^2}{\omega(\omega^2 + \omega'^2)} \right). \end{aligned} \tag{2.40}$$

The full effective action written in terms of double integrals and frequency ω is then

$$\begin{aligned} S_{\text{eff}}[Q(\omega)] =& \frac{1}{2\pi} \int_{-\infty}^{\infty} d\omega' \frac{1}{2} M\omega'^2 Q(\omega') Q(-\omega') + S_V \\ &+ \frac{1}{2\pi^2} \int_{-\infty}^{\infty} d\omega' \int_0^{\infty} d\omega Q(\omega') Q(-\omega') J(\omega) \left\{ \frac{\omega'^2}{\omega(\omega^2 + \omega'^2)} \right\} \end{aligned} \tag{2.41}$$

where S_V is the Fourier transform of $V(q)$. After determining the spectral density, we can use Eq. 2.41 to fully determine the propagator for the paths the particle takes inside a

well, or as was discussed previously, the Green's function for the particle that is localized to a surface before it finally leaves at the point x_σ.

2.3.2 Path Integral in the Classically Forbidden Region

In this section we will use instanton techniques to determine the restricted Green's function which includes all paths that do not cross the enclosed surfaces Σ_i and $\Sigma_{i'}$ where i and i' are labels for different sites. We will provide the main results of the instanton technique here as a detailed explanation can be found in [7] and [8]. In the instanton method, the tunneling amplitude Γ is defined as

$$\Gamma = A\exp(-B/\hbar), \tag{2.42}$$

where the factors A and B are

$$A = \left(\frac{B}{2\pi\hbar}\right)^{1/2}\left|\frac{\det\hat{D}_0}{\det'\hat{D}_1}\right|^{1/2}, \tag{2.43}$$

$$B = \int_0^T\left\{\frac{1}{2}M\dot{q}^2 + V(q)\right\}d\tau + \frac{1}{2}\int_{-\infty}^{\infty}d\tau'\int_{-\infty}^{T}d\tau\alpha(\tau-\tau')\{q(\tau)-q(\tau')\}^2. \tag{2.44}$$

The quantities $\hat{D}_0$ and $\hat{D}_1$ are differential operators and are defined as

$$\hat{D}_0 \equiv \left(-\frac{d^2}{d\tau^2}+\omega^2\right) + \frac{1}{M}\int_{-\infty}^{\infty}\alpha(\tau-\tau')[q(\tau)-q(\tau')]d\tau', \tag{2.45}$$

$$\hat{D}_1 \equiv \left(-\frac{d^2}{d\tau^2}+\frac{1}{M}V''|\bar{q}(\tau)|\right) + \frac{1}{M}\int_{-\infty}^{\infty}\alpha(\tau-\tau')[q(\tau)-q(\tau')]d\tau' \tag{2.46}$$

and the prime on the determinant indicates that the zero eigenvalue is removed.

The above results are obtained by noting that the path integral is dominated by the stationary or critical points of the action. The stationary point or classical path, denoted $\bar{q}(\tau)$, satisfies the equations of motion so that the first variational derivative of the action $\frac{\delta S}{\delta\bar{q}} = 0$. The classical path $\bar{q}(\tau)$ satisfies the boundary conditions such that $q(-T/2) = q_\sigma^{(i)}$ and $q(T/2) = q_\sigma^{(i')}$ during time T. While the classical path dominates, small fluctuations can contribute to the path integral which are given by the second variational derivative of the action. These can be represented by the differential operators mentioned above. In Callan and Coleman's description of the instanton method, multiple "bounces" may take place in which the particle travels back and forth across the barrier. Here, we are only interested in one bounce or one instanton.

The restricted Green's function in the forbidden region is expressed as

$$g_{ii'}(q_\sigma^{(i)}, q_\sigma^{(i')}, \tau) = \int\mathcal{D}q(\tau)e^{-S_E[q(\tau)]/\hbar} \tag{2.47}$$

where $q_\sigma^{(i)}$ is the point at which the particle exits the surface Σ_i and never returns, $q_\sigma^{(i')}$ is the point at which the particle enters the surface $\Sigma_{i'}$, τ represents imaginary time and S_E is the Euclidean action. For one bounce, the restricted Green's function takes the form

$$g(q_\sigma^{(i)}, q_\sigma^{(i')}, \tau) = NT \left(\frac{B}{2\pi\hbar}\right)^{1/2} e^{-B/\hbar} (\det{}'[\hat{D}_1])^{-1/2}. \tag{2.48}$$

We now have the amplitudes for each region and may determine the total Green's function using the propagators found in subsections 2.3.1 and 2.3.2. In the next section, we will determine the spectral densities by employing a dual coupling polaron model.

2.4 Polaron Model

So far we have discussed the PDX formalism, the effective action for a particle coupled to a phonon bath and have determined the propagators that may be used for the classically allowed and forbidden regions. In this section, we will now determine the diagonal and non-diagonal couplings that will be used to determine the spectral density for the particle as it travels in a multiwell potential landscape. These couplings can be determined by using the Holstein and Peierls coupling. A dual coupling model will be discussed in this section which combines both the Holstein and Su-Schrieffer-Heeger model.

2.4.1 Dual Coupling Model

The coupling between electrons and phonons has been well-studied for decades as the interaction leads to various interesting phenomena. An electron traveling through a solid can lead to the formation of a polaron, which is an electron surrounded by a cloud of optical or acoustic phonons. Polarons are interesting subjects as they can be used to determine the physics of various insulating and semiconducting materials. Most models used to describe the coupling between electrons and phonons generally look at diagonal couplings, such as the Holstein model. However, recent studies indicate that off-diagonal couplings may also contribute significantly to polaron properties and their dynamics ([31], [32]). In this thesis we will look at a dual coupling model which includes both Holstein and Peierls coupling, following the prescriptions set forth in [32].

The interaction of electrons and phonons can be represented by the Hamiltonian below:

$$H_0 = -\sum_{ij} t_{ij}(\{b_\lambda\})(c_i^\dagger c_j + c_j^\dagger c_i) + \sum_i \epsilon_i(\{b_\lambda\}) c_i^\dagger c_i + \sum_\lambda \omega_\lambda b_\lambda^\dagger b_\lambda. \tag{2.49}$$

The above Hamiltonian represents a particle hopping between different lattice sites i, j with a hopping amplitude of t_{ij}. The particle interacts with a bath of phonons with frequencies ω_λ where the index λ describes the quantum numbers of the phonons (e.g. $\lambda = \{\vec{q}, \mu\}$). Both the hopping amplitude and the onsite energies are dependent on the

bosonic variables through the displacement operator, $\hat{x}_\lambda = \sqrt{\frac{\hbar}{2M\omega_0}}\left(b_\lambda + b_\lambda^\dagger\right)$. One can expand the onsite and hopping energies in terms of the bosonic variables. The onsite energy can then be given as:

$$\epsilon_i = \epsilon_0 + \sum_\lambda U_i^{(1)}(\lambda)(b_\lambda + b_\lambda^\dagger) + \sum_{\lambda,\lambda'} U_i^{(2)}(\lambda,\lambda')(b_\lambda + b_\lambda^\dagger)(b_{\lambda'} + b_{\lambda'}^\dagger) + ... \tag{2.50}$$

where the quantities $U_i^{(1)}$ and $U_i^{(2)}$ represent the 1-phonon and 2-phonon diagonal couplings. The hopping terms may also be expanded, although its expansion is quite different from the onsite energies. As the hopping amplitudes t_{ij} represent the electron tunneling amplitudes, it will vary as an exponential function of the bosonic variables. The hopping energy can then be written as

$$t_{ij}(\{b_\lambda) = t_0 \exp\left[-\sum_\lambda \frac{V_{ij}(\lambda)}{\omega_\lambda}(b_\lambda + b_\lambda^\dagger)\right] \tag{2.51}$$

$$= t_0\left[1 - \sum_\lambda \frac{V_{ij}(\lambda)}{\omega_\lambda}(b_\lambda + b_\lambda^\dagger)\right] \tag{2.52}$$

where we have expanded the exponential and kept the linear coupling. We can now see how the displacement operators affect the diagonal and off-diagonal couplings. In the onsite energy, the diagonal terms come from the polarization of the lattice by the electron. For the hopping energy, the phonons modify the distance between lattice sites as they vibrate which in turn modulates the tunneling amplitude required by the electron to travel between sites.

To study the Hamiltonian we will first take its Fourier transform and make a few simplifying approximations. We will only include linear couplings of the electron to the phonons and only consider the optical branch. The Fourier transform for the creation operator is

$$c_{\mathbf{k}}^\dagger = \frac{1}{\sqrt{N}} \sum_{\mathbf{r}_i} e^{-i\mathbf{k}\cdot\mathbf{r}} c_i(\mathbf{r}_i) \tag{2.53}$$

and the Fourier transform for the Hamiltonian is then

$$H = \sum_{\mathbf{k}} \epsilon_{\mathbf{k}} c_{\mathbf{k}}^\dagger c_{\mathbf{k}} + \sum_{\mathbf{q}} \omega_{\mathbf{q}} b_{\mathbf{q}}^\dagger b_{\mathbf{q}} + \frac{1}{\sqrt{N}} \sum_{\mathbf{k},\mathbf{q}} V(\mathbf{k},\mathbf{q}) c_{\mathbf{k-q}}^\dagger c_{\mathbf{k}} (b_{\mathbf{q}}^\dagger + b_{-\mathbf{q}}). \tag{2.54}$$

The quantity $V(\mathbf{k},\mathbf{q})$ is the sum of the Fourier transforms for the diagonal and non-diagonal coupling terms, $c_{\mathbf{k}}^\dagger$ and $b_{\mathbf{q}}^\dagger$ are the creation operators for the electrons and phonons respectively, $\mathbf{k}$ and $\mathbf{q}$ are the momenta for the electron and phonons respectively which are summed over the first Brillouin zone and N is the number of lattice sites where $N \to \infty$.

The interaction term $V(\mathbf{k},\mathbf{q})$ can be split into the diagonal and non-diagonal terms as

$$V(\mathbf{k},\mathbf{q}) = g_1(\mathbf{q}) + g_2(\mathbf{k},\mathbf{q}) \tag{2.55}$$

where the diagonal coupling, $g_1(\mathbf{q})$, is dependent only on the phonon momentum while the non-diagonal coupling, $g_2(\mathbf{k},\mathbf{q})$, depends on both phonon and electron momenta. To study these results, we will use the following properties in our model. We take the lattice constant to be $a = 1$, assume only nearest neighbour hopping ($t_{ij} = t_0\delta_{i\pm1,j}$), and as mentioned previously, we will consider coupling to Einstein phonons only where the frequency $\omega_q = \Omega_0$. The diagonal or non-interacting part of the Hamiltonian is simply

$$H_0 = -2t_0 \sum_{\mathbf{k}} \cos(\mathbf{k}) c^\dagger_{\mathbf{k}} c_{\mathbf{k}} + \sum_{\mathbf{q}} \Omega_0 b^\dagger_{\mathbf{q}} b_{\mathbf{q}} \tag{2.56}$$

where the cosine term comes from the Fourier transformation of the hopping terms $c_i^\dagger c_j + c_j^\dagger c_i$ in the original site Hamiltonian. To determine the couplings between the electron and phonons, we will use the Holstein and Su-Shrieffer-Heeger (SSH) models for the diagonal and non-diagonal couplings respectively. For the diagonal coupling, the Holstein model gives $g_1(\mathbf{q}) = g_0$, a constant with no momentum dependence. In the SSH model we modify the hopping element slightly so that the hopping amplitude becomes

$$t_{i,i+1} = t_0 - \alpha_0(\hat{x}_{i+1} - \hat{x}_i), \tag{2.57}$$

where $\hat{x}_i$ is the displacement operator. By Fourier transforming the Hamiltonian with this form of the hopping, the non-diagonal coupling $g_2(\mathbf{k},\mathbf{q})$ is

$$g_2(\mathbf{k},\mathbf{q}) = 2i\alpha_0[\sin(\mathbf{k}-\mathbf{q}) - \sin(\mathbf{k})]. \tag{2.58}$$

We now have the complete form of the Hamiltonian for the dual coupling model. The Hamiltonian for a particle interacting with a bath of phonons with diagonal and non-diagonal couplings included is

$$H = -2t_0 \sum_{\mathbf{k}} \cos(\mathbf{k}) c^\dagger_{\mathbf{k}} c_{\mathbf{k}} + \sum_{\mathbf{q}} \Omega_0 b^\dagger_{\mathbf{q}} b_{\mathbf{q}} + \frac{1}{\sqrt{N}} \sum_{\mathbf{k},\,\mathbf{q}} (g_0 \tag{2.59}$$

$$+ \frac{2i}{\sqrt{N}}\alpha_0[\sin(\mathbf{k}-\mathbf{q}) - \sin(\mathbf{k})]\Big) c^\dagger_{\mathbf{k}-\mathbf{q}} c_{\mathbf{k}} (b^\dagger_{\mathbf{q}} + b_{-\mathbf{q}}). \tag{2.60}$$

We can define the adiabaticity parameter as $\Lambda_0 = \Omega_0/t_0$. When $\Lambda_0 \ll 1$, then the electron dynamics are fast while the phonon dynamics are slow.

The model described above is one of the simplest models one can study to determine the dynamics of a polaron with diagonal and off-diagonal couplings. Together with the Auerbach and Kivelson PDX method, we will use this model to determine the full Green's

function for a particle coupled to a bosonic bath tunneling between multiple wells. We will first study the Holstein and SSH models separately to determine how the combined model with both couplings will affect the particle dynamics.

2.4.2 The Holstein and Su-Schrieffer Heeger Models

In the Holstein model, the Hamiltonian contains only the constant coupling between the electrons and phonons giving it the following form:

$$H = -t \sum_{<i,j>} (c_i^\dagger c_j + c_j^\dagger c_i) + \Omega_0 \sum_i b_i^\dagger b_i + g \sum_i c_i^\dagger c_i (b_i^\dagger + b_i), \tag{2.61}$$

which in momentum space is

$$H = \sum_{\mathbf{k}} \epsilon_{\mathbf{k}} c_{\mathbf{k}}^\dagger c_{\mathbf{k}} + \Omega_0 \sum_{\mathbf{q}} b_{\mathbf{q}}^\dagger b_{\mathbf{q}} + \frac{g}{\sqrt{N}} \sum_{\mathbf{k},\mathbf{q}} c_{\mathbf{k}-\mathbf{q}}^\dagger c_{\mathbf{k}} (b_{\mathbf{q}}^\dagger + b_{-\mathbf{q}}). \tag{2.62}$$

In a system with only diagonal couplings, phonons can only be created and absorbed when an electron stays on the same site. In the weak coupling limit, the coupling term can be treated as a perturbation. With $g = 0$, the eigenstates and eigenenergies of the Hamiltonian are simply:

$$c_{\mathbf{k}}^\dagger |0\rangle \qquad c_{\mathbf{k}-\mathbf{q}}^\dagger b_{\mathbf{q}}^\dagger |0\rangle \qquad c_{\mathbf{k}-\mathbf{q}-\mathbf{q}'}^\dagger b_{\mathbf{q}}^\dagger b_{\mathbf{q}'}^\dagger |0\rangle \qquad c_{\mathbf{k}-\mathbf{q}-\mathbf{q}'-\mathbf{q}''}^\dagger b_{\mathbf{q}}^\dagger b_{\mathbf{q}'}^\dagger b_{\mathbf{q}''}^\dagger |0\rangle \qquad ... \tag{2.63}$$

$$\epsilon_{\mathbf{k}} \qquad \epsilon_{\mathbf{k}-\mathbf{q}} + \Omega_0 \qquad \epsilon_{\mathbf{k}-\mathbf{q}-\mathbf{q}'} + 2\Omega_0 \qquad \epsilon_{\mathbf{k}-\mathbf{q}-\mathbf{q}'-\mathbf{q}''} + 3\Omega_0 \qquad ... \tag{2.64}$$

where $\epsilon_{\mathbf{k}} = -2t \sum_{i=1}^{d} \cos \mathbf{k}_i$ and $d = 1, 2, 3$. The higher energy states will contain one electron and n phonons. The effect of the phonons will be to narrow the band of the energy spectrum and shift it vertically, however, the energy spectrum will still maintain a cosine form. If the coupling g is turned on, the free electron state can mix with the higher energy states above it.

In the strong coupling limit, it is the hopping term that becomes the perturbation. One can use the Lang-Firsov canonical transformation ([25]) in order to diagonalize the second and third term in the Hamiltonian. Then the small polaron energy up to first order is

$$E_{\mathbf{k}} = -\frac{g^2}{\Omega_0} - \exp\left(-\frac{g^2}{\Omega_0^2}\right) 2t \sum_{i=1}^{d} \cos(\mathbf{k}_i) \tag{2.65}$$

where we have taken into account the energy mediated by the quantities $c_i^\dagger c_j$. We see that up to first order the energy spectrum still takes the form of a tight binding model but the bandwidth is exponentially suppressed and shifted by $-g^2/\Omega_0$.

In the SSH model, the coupling between the electron and phonons are off-diagonal.

Recall that the Hamiltonian for this model is

$$H = \sum_{k} \epsilon_{\mathbf{k}} c^{\dagger}_{\mathbf{k}} c_{\mathbf{k}} + \Omega_0 \sum_{\mathbf{q}} b^{\dagger}_{\mathbf{q}} b_{\mathbf{q}} + \frac{1}{\sqrt{N}} \sum_{\mathbf{k},\mathbf{q}} g(\mathbf{k},\mathbf{q}) c^{\dagger}_{\mathbf{k}-\mathbf{q}} c_{\mathbf{k}} (b^{\dagger}_{\mathbf{q}} + b_{\mathbf{q}}) \tag{2.66}$$

where $g(\mathbf{k},\mathbf{q}) = 2i\alpha_0[\sin(\mathbf{k}-\mathbf{q}) - \sin(\mathbf{k})]$ and represents the off-diagonal coupling.

In the Holstein model, the effective hopping terms are exponentially suppressed when there are diagonal couplings between the electron and phonons. Here, the non-diagonal couplings allow the particle to hop to a neighbouring site, create a phonon, and then hop to the next site while absorbing the phonon that was created in the previous site. The non-diagonal couplings then mediate the hopping of the particle from site to site. These couplings can be used to calculate the spectral function, $J(\omega)$.

2.4.3 Spectral densities of the Holstein and SSH Polarons

In this subsection, we will calculate the spectral densities of the Holstein and SSH polarons which can be inserted into the effective action as determined by Caldeira-Leggett. The purpose of this is to include the diagonal and non-diagonal couplings into the path integral formalism devised by Auerbach and Kivelson. By including these couplings, we can then create a more realistic model for biological and chemical reactions.

The spectral density is defined as

$$J(\omega) = \frac{\pi}{2} \sum_{\mathbf{q}} \frac{|c_{\mathbf{q}}|^2}{m_{\mathbf{q}} \omega_{\mathbf{q}}} \delta(\omega - \omega_{\mathbf{q}}) \tag{2.67}$$

where $|c_q|^2$ is the coupling, m_q is the phonon mass and ω_q is the phonon frequency. To determine the spectral density for the Holstein and SSH models, we first have to examine the interactions between the particle and phonons. We will begin with the Holstein model before moving onto the SSH model.

2.4.4 Diagonal Coupling

The spectral density for the diagonal coupling begins by starting with

$$c_{\mathbf{q}} = \frac{g_0}{\sqrt{N}} \delta(\omega - \omega_{\mathbf{q}}), \tag{2.68}$$

which can be inserted into the spectral density. As we are only coupling the particle to optical phonons, the Einstein model is used to approximate the phonon frequency, $\omega_{\mathbf{q}}$, as

Ω_0. The spectral density then takes the following form

$$J(\omega) = \frac{\pi}{2}\sum_q \frac{g_0^2}{Nm\Omega_0}\delta(\omega-\Omega_0) \tag{2.69}$$

$$= \frac{\pi}{2}\frac{g_0^2}{m\Omega}\delta(\omega-\Omega_0) \tag{2.70}$$

where the sum over the delta function gives N times the delta function. Generalizing this to d dimensions provides the following result

$$J(\omega) = \frac{\pi}{2}\frac{g_0^2 d}{m\Omega_0}\delta(\omega-\Omega_0). \tag{2.71}$$

2.4.5 Non-diagonal Coupling

The spectral density using the non-diagonal coupling is determined similarly to the diagonal coupling although it is slightly more involved. The coupling here is

$$g(\mathbf{k},\mathbf{q}) = \frac{2i}{\sqrt{N}}\alpha_0[\sin(\mathbf{k}-\mathbf{q})-\sin(\mathbf{k})]^2\delta(\omega-\Omega_0), \tag{2.72}$$

which is dependent on $\mathbf{k}$, the momentum of the particle. The spectral density in 1D is then

$$J_k^{(1D)}(\omega) = \frac{\pi}{2}\sum_q \frac{|g(k,q)|^2}{m\Omega}\delta(\omega-\Omega) \tag{2.73}$$

$$= \frac{\pi}{2}\sum_q \frac{4}{N}\frac{[\sin(k-q)-\sin(k)]^2}{m\Omega}\delta(\omega-\Omega) \tag{2.74}$$

$$= \frac{\pi}{2}\alpha_0^2\int_{-\pi}^{\pi}\frac{dq}{2\pi}\frac{4}{Nm\Omega}\{\sin^2(k-q)-2\sin(k-q)\sin(k)+\sin^2(k)\}\delta(\omega-\Omega) \tag{2.75}$$

$$= \frac{\pi\alpha_0^2}{m\Omega}(1+2\sin^2(k))\delta(\omega-\Omega). \tag{2.76}$$

Similar calculations can be done in 2D and 3D by taking into account the vector components. In the 2D and 3D case, the coupling takes the following form.

$$c_q^{(2D)} = \frac{2i}{\sqrt{N}}\alpha_0[\sin(k_x-q_x)+\sin(k_y-q_y)-\sin(k_x)-\sin(k_y)]^2\delta(\omega-\Omega) \tag{2.77}$$

$$c_q^{(3D)} = \frac{2i}{\sqrt{N}}\alpha_0\left[\sin(k_x-q_x)+\sin(k_y-q_y)+\sin(k_z-q_z)\right. \tag{2.78}$$

$$\left.-\sin(k_x)-\sin(k_y)-\sin(k_z)\right]^2\delta(\omega-\Omega) \tag{2.79}$$

The integration for the 2D spectral density can then be carried out as follows

$$\begin{aligned}
J_{\mathbf{k}}^{(2D)}(\omega) &= \frac{\pi}{2}\frac{4\alpha_0^2}{Nm\Omega}\sum_q \{\sin(k_x-q_x)+\sin(k_y-q_y)-\sin(k_x)-\sin(k_y)\}^2\delta(\omega-\Omega) \\
&= \frac{\pi}{2}\frac{4\alpha_0^2}{m\Omega}\frac{1}{(2\pi)^2}\int_{-\pi}^{\pi}dq_x\int_{-\pi}^{\pi}dq_y\left\{\sin^2(k_x-q_x)+2\sin(k_x-q_x)\sin(k_y-q_y)\right. \\
&\quad -2\sin(k_x-q_x)\sin(k_x)-2\sin(k_x-q_x)\sin(k_y)+\sin^2(k_y-q_y) \\
&\quad -2\sin(k_y-q_y)\sin(k_x)-2\sin(k_y-q_y)\sin(k_y) \\
&\quad \left.+\sin^2(k_x)+2\sin(k_x)\sin(k_y)+\sin^2(k_y)\right\} \\
&= \frac{\pi}{2}\frac{4\alpha_0^2}{m\Omega}(1+\sin^2(\mathbf{k})\delta(\omega-\Omega) \\
&= \frac{\pi\alpha_0^2}{m\Omega}(2+2\sin^2(\mathbf{k})\delta(\omega-\Omega).
\end{aligned} \tag{2.80}$$

The same calculation in 3D can be carried out and it yields

$$J_{\mathbf{k}}^{(3D)}(\omega) = \frac{\pi\alpha_0^2}{m\Omega}(3+2\sin^2(\mathbf{k})\delta(\omega-\Omega). \tag{2.81}$$

The spectral density then gives this general form for $d = 1$, 2 and 3 dimensions

$$J_{\mathbf{k}}^{(d)}(\omega) = \frac{\pi\alpha_0^2}{m\Omega}(d+2\sin^2(\mathbf{k}))\delta(\omega-\Omega). \tag{2.82}$$

In this last spectral function, we note that it not only depends on frequency, ω, but also on the electron momentum k. As a result, the effective action in which this spectral function is inserted into, will also be dependent on the electron momentum.

2.4.6 Fourier Transform of the Effective Action

As seen previously, the full effective action written in terms of double integrals using ω is

$$\begin{aligned}
S_{\text{eff}}[Q(\omega)] =& \frac{1}{2\pi}\int_{-\infty}^{\infty}d\omega\frac{1}{2}M\omega^2Q(\omega)Q(-\omega)+S_V \\
&+\frac{1}{2\pi^2}\int_{-\infty}^{\infty}d\omega\int_0^{\infty}d\omega' Q(\omega)Q(-\omega)J(\omega')\frac{\omega^2}{\omega'(\omega'^2+\omega^2)}
\end{aligned} \tag{2.83}$$

where S_V is the Fourier transform of $V(q)$ defined as

$$S_V(Q(\omega)) \equiv \int_{-\infty}^{\infty}d\tau V(q(\tau)). \tag{2.84}$$

The effective actions written as integrals over time and frequency for the diagonal cou-

pling are

$$S_{\text{eff}}[q(\tau)] = \int_{-\infty}^{\infty} \left\{ \frac{1}{2} M\dot{q}^2 + V(q) \right\} d\tau + \frac{1}{2} \int_{-\infty}^{\infty} d\tau' \int_{-\infty}^{\infty} d\tau \frac{g_0^2 d}{4m\Omega} e^{-\Omega|\tau-\tau'|} \{q(\tau) - q(\tau')\}^2 \Theta(\Omega), \tag{2.85}$$

$$S_{\text{eff}}[Q(\omega)] = \frac{1}{2\pi} \int_{-\infty}^{\infty} d\omega \frac{1}{2} M\omega^2 Q(\omega) Q(-\omega) + S_V + \frac{1}{2\pi^2} \int_{-\infty}^{\infty} d\omega Q(\omega) Q(-\omega) \frac{\pi d g_0^2}{2m\Omega^2} \frac{\omega^2}{(\Omega^2 + \omega^2)} \Theta(\Omega) \tag{2.86}$$

and for the non-diagonal coupling are

$$S_{\text{eff}}[q(\tau)] = \int_{-\infty}^{\infty} \left\{ \frac{1}{2} M\dot{q}^2 + V(q) \right\} d\tau + \frac{1}{2} \int_{-\infty}^{\infty} d\tau' \int_{-\infty}^{\infty} d\tau \frac{\alpha_0^2}{2m\Omega} \times (d + 2\sin^2(\mathbf{k})) e^{-\Omega|\tau-\tau'|} \{q(\tau) - q(\tau')\}^2 \Theta(\Omega), \tag{2.87}$$

$$S_{\text{eff}}[Q(\omega)] = \frac{1}{2\pi} \int_{-\infty}^{\infty} d\omega \frac{1}{2} M\omega^2 Q(\omega) Q(-\omega) + S_V + \frac{1}{2\pi^2} \int_{-\infty}^{\infty} d\omega Q(\omega) Q(-\omega) \frac{\pi \alpha_0^2}{m\Omega^2} \frac{\omega^2}{(\Omega^2 + \omega^2)} (d + 2\sin^2(\mathbf{k})) \Theta(\Omega). \tag{2.88}$$

Here we note that the effective action with the non-diagonal coupling is dependent on the particle momentum $\mathbf{k}$.

Given that we have all of the pieces for determining the path integrals, we can now determine the expressions for the propagators in the classically allowed and forbidden regions. The propagator for the particle in the classically allowed region (or inside a potential well) is

$$g_i(E) = \prod_j \frac{1}{2} \text{cosech} \left(\frac{\omega_j T}{2} \right) \int_{q_i}^{q_{\sigma,i}} \mathcal{D}q(\tau) \exp \left(\frac{i}{\hbar} \int_{-\infty}^{\infty} \left\{ \frac{1}{2} M\dot{q}^2 + V(q) \right\} d\tau + \frac{1}{2} \int_{-\infty}^{\infty} d\tau' \int_{-\infty}^{\infty} d\tau \frac{g_0^2 d}{4m\Omega} e^{-\Omega|\tau-\tau'|} \{q(\tau) - q(\tau')\}^2 \Theta(\Omega) \right), \tag{2.89}$$

while the propagator for a particle in the forbidden region is

$$g_{ij}(E) = \left(\frac{B}{2\pi\hbar} \right)^{1/2} \left| \frac{\det \hat{D}_0}{\det' \hat{D}_1} \right|^{1/2} \int_{q_{\sigma,i}}^{q_{\sigma,j}} \mathcal{D}q(\tau) \exp \left(\int_{-\infty}^{\infty} \left\{ \frac{1}{2} M\dot{q}^2 + V(q) \right\} d\tau + \frac{1}{2} \int_{-\infty}^{\infty} d\tau' \int_{-\infty}^{\infty} d\tau \frac{\alpha_0^2}{2m\Omega} (d + 2\sin^2(\mathbf{k})) e^{-\Omega|\tau-\tau'|} \{q(\tau) - q(\tau')\}^2 \Theta(\Omega) \right) \tag{2.90}$$

where

$$B = \int_0^T \left\{ \frac{1}{2} M \dot{q}^2 + V(q) \right\} d\tau + \frac{1}{2} \int_{-\infty}^{\infty} d\tau' \int_{-\infty}^{T} d\tau \alpha(\tau - \tau') \{q(\tau) - q(\tau')\}^2, \tag{2.91}$$

$$\hat{D}_0 \equiv \left(-\frac{d^2}{d\tau^2} + \omega^2 \right) + \frac{1}{M} \int_{-\infty}^{\infty} \alpha(\tau - \tau')[q(\tau) - q(\tau')] d\tau', \tag{2.92}$$

$$\hat{D}_1 \equiv \left(-\frac{d^2}{d\tau^2} + \frac{1}{M} V''|\bar{q}(\tau)| \right) + \frac{1}{M} \int_{-\infty}^{\infty} \alpha(\tau - \tau')[q(\tau) - q(\tau')] d\tau'. \tag{2.93}$$

These expressions for the propagators can then be inserted into the Auerbach and Kivelson PDX formalism in order to determine the total Green's function for a particle that starts at some site i and then ends at site i'. The following equations which were provided in earlier sections can then be fully determined:

$$t_{ij} = [\Sigma_i] g_{ij} [\Sigma_j] \tag{2.94}$$

$$T_{ij} = t_{ij} + t_{im} \mathcal{G}_{mn} t_{nj} \tag{2.95}$$

$$\mathcal{G}_{ij} = g_i \delta_{ij} + g_i T_{ij} g_j \tag{2.96}$$

where the flux operator $[\Sigma_i]$ was defined as

$$[\Sigma_i] = \lim_{x, x' \to x_{\sigma,i}} \int_{\Sigma_i} d\sigma \left| x_{\sigma,i} \right\rangle \left\langle x \right| \left[\frac{\hbar}{2m} \vec{\nabla}_\sigma \right] \left| x' \right\rangle \left\langle x_{\sigma,i} \right|. \tag{2.97}$$

In summary, we have determined the tunneling amplitude for a particle coupled to a phonon bath in a multiwell potential. Despite being coupled to a phonon bath, one can trace over the environment and determine the environment's effects on the system. Previous work done to determine the tunneling amplitude of a particle coupled to a phonon bath required the use of truncation methods which introduced artificial cutoffs. By using the PDX formalism, we were able to avoid this by deconstructing the potential energy landscape into simpler pieces where each region could be solved using different methods. The full Green's function could then be determined using the connection formula constructed by Auerbach and Kivelson. By constructing and solving the problem in this way, we have prepared a model to describe a particle coupled to a phonon bath traveling in a multiwell potential.

Chapter 3

Experimental Setup and Results

The objective of this experiment was to determine whether the deuteration of molecules could affect the binding of a ligand to its receptor. Previous studies had shown that a possible molecular vibration-sensing mechanism was involved in olfaction for fruit flies. Our experiment was designed to determine quantitatively whether such a mechanism was present in other GPCR systems. The β_1 and β_2 adrenergic receptor system, the agonist epinephrine and its deuterated counterparts were chosen to study these effects as the β-AR system is well-studied.

Our experiment studied the effects that non-deuterated and deuterated epinephrine compounds had on the production of cAMP. A quantitative analysis was performed by using an enzyme-linked immunosorbent assay (ELISA) to determine the levels of cAMP. Our experimental results, however, were very inconsistent and troubleshooting indicated the possibility that the preparation of the agonists was not suitable for our experiment. For this reason, we were not able to establish any definite conclusions from the experiments. A detailed explanation of the experimental setup and a discussion of the results are provided in this chapter.

3.1 Materials and Methods

The agonist epinephrine was chosen for this experiment, as it is a known agonist for the β-AR system. To avoid differences in compound and sample preparation, all agonists were purchased from the same company in the same form. Epinephrine, epinephrine-d_3 and epinephrine-d_6 (see Fig. 3.1) were all purchased from Medical Isotopes Inc. in powder form and were dissolved in 100% Dimethyl sulfoxide (DMSO). Epinephrine is soluble in hydrochloric acid (HCl) but DMSO was used instead as it was unknown whether the addition of acid would negatively affect cell growth. DMSO is a universal solvent as it dissolves both polar and nonpolar compounds. All agonists were dissolved in the lowest volume of DMSO possible to maintain low concentrations of DMSO in the final volume of growth medium.

HEK293 cells (derived from human embryonic kidney cells) were introduced to DNA that coded for either β_1ARs, $\beta_2 ARs$ or both. This process of deliberately introducing DNA to the cell, called transfection, allows the cells to take up the DNA and express these β-adrenergic receptors. The cells were cultured in Dulbecco's Modified Eagle Medium (DMEM), a liquid or gel that contains substances required to support cell growth such as

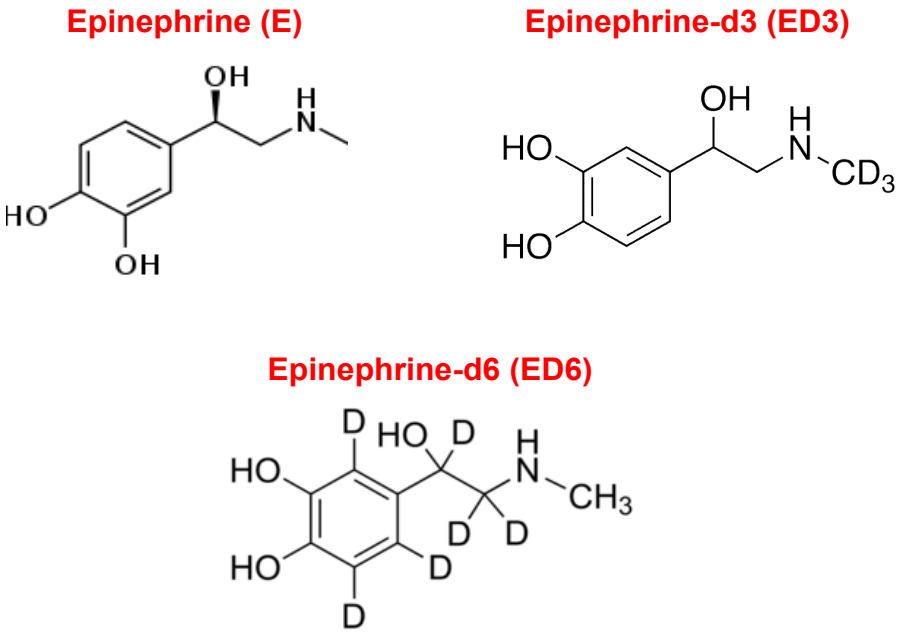

Figure 3.1: Chemical structures of epinephrine, epinephrine-d_3 and epinephrine-d_6. Epinephrine-d_3 has protons on the methyl group replaced with deuterium. Epinephrine-d_6 has all protons attached to carbon molecules switched with deuterium except the lone methyl group.

glucose and amino acids. Cells were grown until 90-100% of the plate surface was covered in adhered cells. Two controls were used in this experiment: a sample treated with only 3-isobutyl-1-methylxanthine (IBMX) and a sample treated with only Forskolin (FSK). The first control served as a negative control as IBMX prevents the degradation of cAMP. The second control acted as a positive control as it maximally stimulates cAMP production. Forskolin also activates adenylyl cyclase directly and not through a G protein-dependent pathway [26, 35].

Cells were treated with G_i or G_s inhibitors before treatment with agonists to block the α_i or α_s subunit function. The G_i inhibitor used was pertussis toxin and the G_s inhibitors were either mellitin or G protein antagonist peptide (GPAP). Pertussis toxin was added to the cells 16 hours before treatment with agonist and G_s inhibitors were added to cells 2 hours before treatment. The purpose of these inhibitors was to determine if the coupling of the receptor to specific α subunits affected cAMP production.

Cells were treated with varying concentrations of epinephrine or deuterated epinephrine for 30 minutes and then destroyed and lysed with lysis buffer. They were further sonicated (agitated at high frequencies using sound energy) for 5 seconds to ensure cells had been ruptured. Samples were centrifuged at 2500rpm for 5 minutes at 4°C to separate the

cellular debris from the cellular solution which contained the cAMP and other proteins. Cell debris was discarded and a Bradford protein assay was performed on the remaining samples. The Bradford assay was done to determine the total concentration of protein (μg/μL) in the samples. Samples were then diluted and normalized down to the sample with the lowest protein concentration. This ensured that differences in cAMP production were due to agonist efficacy and not due to a difference in the amount of protein or cellular content in each sample.

The cyclic AMP assay kit, purchased from Cell Signaling, is a competition enzyme-linked immunosorbent assay (ELISA) that utilizes antibodies and colour changes on a 96-well plate to determine the concentration and identity of a substance. The 96 well-plate was coated with immobilized rabbit antibodies which identify and bind to cAMP. 50μL of each prepared sample was added to the plate in triplicate. 50μL of HRP-linked cAMP (cAMP bound to horse radish peroxidase enzyme) was also added to each well containing a sample. Standard samples with known concentrations of cAMP could also added to the plate. Depending on the availability of space in the plate, the standard samples were not always included. The cAMP in our sample and the HRP-linked cAMP compete with each other in binding to the antibodies in the plate. The plate was left to incubate at room temperature for 3 hours on a plate shaker to ensure proper mixing of all solutions.

After incubation, the wells were washed three times with a wash buffer to remove any excess cAMP (both the sample cAMP and the HRP-linked cAMP) not bound to the antibodies. A substance called TMB substrate was then added. TMB substrate is a compound acted on by the HRP enzyme in the HRP-linked cAMP. The interaction between the TMB substrate and the HRP enzyme induces a colour change that can be detected via spectroscopy. Wells that showed an intense colour change indicated that there was much more HRP-linked cAMP bound to the antibodies than the cAMP obtained from the cell. It also implied that there was a smaller concentration of cAMP in the sample. A less intense colour change indicated that the samples had a much higher concentration of cAMP. The colour change was analyzed using a spectrophotometer and the absorbance of each sample at 450nm was read.

The biological response, or the percentage of activity as we call it here, is the production of cAMP. The percentage of activity, as defined by the manufacturer, was calculated as follows:

$$100 \times \frac{A - A_{basal}}{A_{max} - A_{basal}} \tag{3.1}$$

where A is the absorbance of the sample, A_{basal} is the absorbance of the sample with the basal level of cAMP, and A_{max} is the absorbance of the sample with the highest amount of cAMP. The values for A_{basal} and A_{max} were provided by the control samples treated with IBMX and FSK respectively. The absorbance spectrum of each sample gives an indication of how much cAMP is present. The quantity $A_{max} - A_{basal}$ thus should give the total range of cAMP produced in the experiment. The percentage of activity as defined above in Eq.

3.1 thus gives the relative increase or decrease of cAMP compared to the basal level.

3.2 Results

The first assay was used to determine the concentration range that should be used for subsequent experiments. Epinephrine, epinephrine-d_3 (ED3) and epinephrine-d_6 (ED6) were used to treat cells at concentrations of 10nM, 100nM and 1μM. These concentrations were chosen as previous experiments showed that concentrations of epinephrine in this range produced significant levels of cAMP [16, 30]. The treatments were performed on cells with either β_1 or β_2 adrenergic receptors. The results of the first assay indicated that concentrations between 100nM and 1μM would provide optimal results so concentrations within this range were used for the following assays (Fig. 3.2 to 3.4). The treatment with FSK also indicated that concentrations in the micromolar range would most likely saturate cAMP production (Fig. 3.5 and 3.6). This first assay also indicated that there were possible differences in efficacy between the three agonists. At a concentration of 1μM, cells with β_1AR and treated with ED3 increased by 9.1% compared to the basal level while agonists epinephrine and ED6 increased production of cAMP by 102.7% and 103.3% respectively. In β_2AR, the percentage increases for epinephrine, ED3 and ED6 were 40.6%, 11.5% and 98.5% respectively.

Assays two and three, which tested all 3 compounds at varying concentrations, indicated that not all of the results were following the dose-response curve that was expected of epinephrine when acting on β-adrenergic receptors. Usually, one should see increasing activity with increasing concentration of agonist until it reaches a point where the activity plateaus. The results showed that the deuterated compounds tended to give results that fluctuated even with increasing concentration (see Fig. 3.7 and 3.8). Many of these results also indicated that the percentage of activity was below 0%, which implied that these samples had levels of cAMP lower than the basal level. Fig. 3.8 could be interpreted as showing the typical dose-response as the percentage of activity does increase with increasing ED6 concentration that peaks at 2.5μM. On the other hand, the results for cells treated with regular epinephrine and the cAMP standard samples were typical of what was seen in the literature (see Fig. 3.9). It is possible that human error contributed to these inconsistencies seen here. However, it is strange that half of the samples worked while the others did not, especially since all samples were prepared at the same time using the same methods. This leads us to believe that there is another issue affecting the results besides human error.

The ensuing assays used pertussis toxin (G_i inhibitor) and melittin or GPAP (G_s inhibitors) to determine if the coupling of the receptor to the G_α subunit was causing the fluctuating results. Previous research showed that high concentrations of cAMP can cause the β-ARs to switch the coupling from G_s to G_i [16, 21, 33, 37]. A switch in coupling to

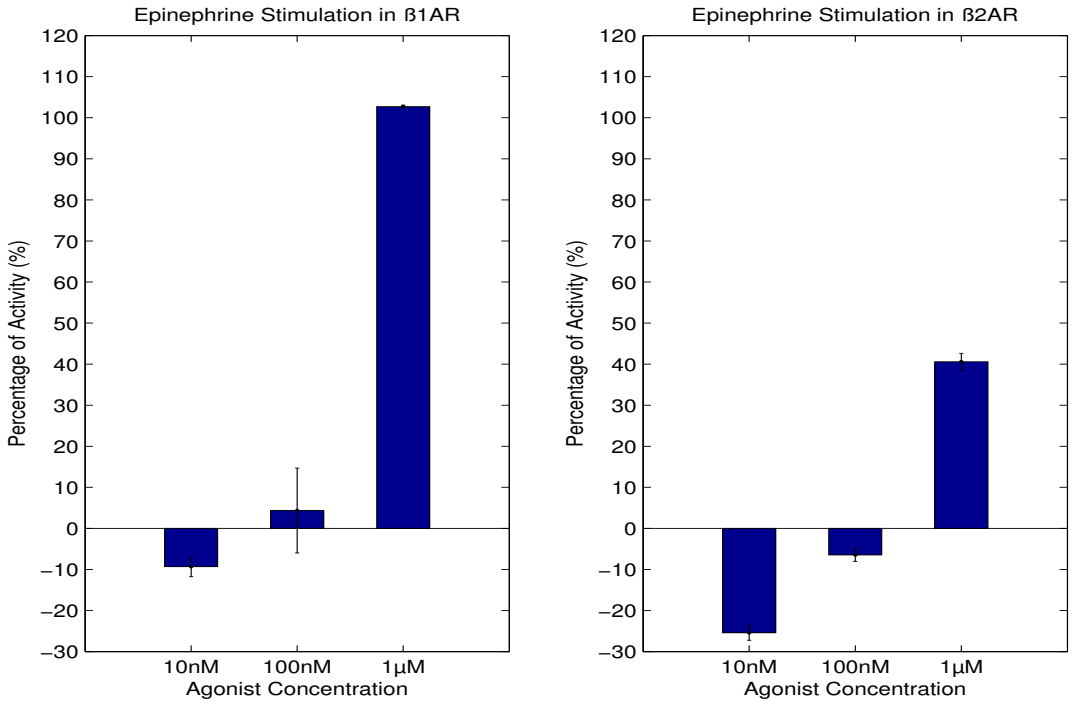

Figure 3.2: Assay 1. Plot of the agonist (epinephrine) concentration versus the percentage of activity (%). HEK293 cells were transfected with either β_1 (left) or β_2 (right) adrenergic receptors at varying concentrations. Results indicated that the percentage of activity increased with increasing epinephrine concentration.

the G_i subunit could inhibit adenylyl cyclase and decrease cAMP production. Pertussis toxin inhibits the G_i subunit by adding a molecule to the G protein. This addition prevents the receptor from interacting with the G protein [20]. Melittin inhibits G_s by reducing its affinity for both GTP and GDP [17]. Lastly, GPAP binds to the region of the G protein that interacts with the receptor which prevents activation [34].

As epinephrine binding to β-adrenergic receptors should stimulate the G_s subunit, adding G_i inhibitor should theoretically not affect the activity of the agonist. Thus, results of cells treated with G_i should give very similar results to those cells with no added inhibitors. In contrast, adding G_s inhibitor should show decreased levels of activity as less cAMP is produced. Assays were performed using these inhibitors and the agonists at varying concentrations to determine if these results would be consistent with what was known in the literature. The results of the assay using epinephrine-d_3 is provided in figures 3.10 to 3.13.

The results for figures 3.10 to 3.14 conflict with what is expected. Firstly, figure 3.10 indicates that the treatment using ED3 without inhibitors gave the trend we were expecting to see in the previous assays (assays 2 and 3), an increasing response with increasing concentration. The results from assay 3 had shown randomly fluctuating levels of activity.

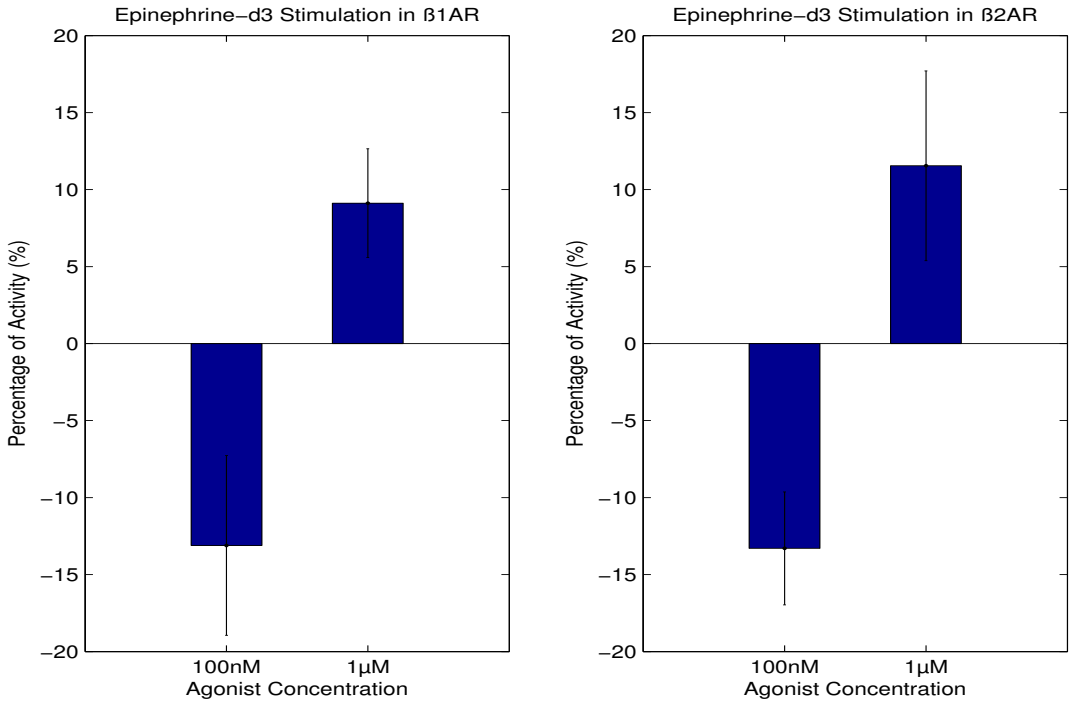

Figure 3.3: Assay 1. Plot of the agonist (epinephrine-d_3) concentration versus the percentage of activity (%). HEK293 cells were transfected with either β_1 (left) or β_2 (right) adrenergic receptors at varying concentrations. Results indicated that the percentage of activity increased with increasing epinephrine-d_3 concentration.

This indicates that there are consistency problems between the experiments that could be unrelated to G_s or G_i coupling. The treatments with the inhibitors also revealed that the inhibitors did not work as we had hoped. While the G_s inhibitor did appear to decrease the activity level of the cells, the cells treated with G_i inhibitor did not show the same dose-response as the cells treated with no inhibitors. These results were in contrast with assay 7 where the G_s inhibitor did hinder cAMP production (Fig. 3.15). The G_s inhibited cells show that cAMP production is decreased by 3-14% compared to the non-inhibited cells.

In general, the results from all assays are very inconsistent. It is difficult to draw any significance from the experiments as they conflict with information gathered from previous studies that also used the β-adrenergic system, epinephrine and HEK293 cells. Also no clear trend can be seen from these results. The initial experiment and some treatments did show the dose-response that agreed with the existing literature. In certain instances, it also appears as if the deuterated and non-deuterated epinephrine are following a bell-shaped curve, where they initially increase with increasing concentration but then slowly decrease in activity after a certain point. However, whether this is a significant outcome or not is doubtful as the results themselves are not stable and do not agree with what

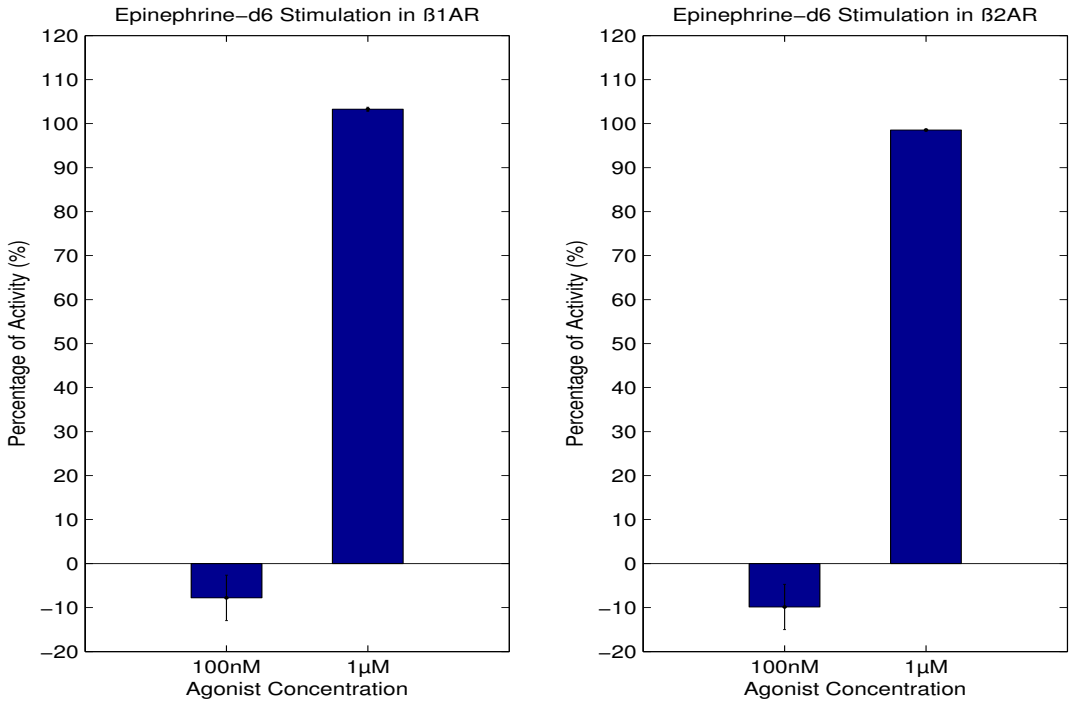

Figure 3.4: Assay 1. Plot of the agonist (epinephrine-d_6) concentration versus the percentage of activity (%). HEK293 cells were transfected with either β_1 (left) or β_2 (right) adrenergic receptors at varying concentrations. Results indicated that the percentage of activity increased with increasing epinephrine concentration.

is expected. These results indicate that there may be a problem with the setup that is causing inconsistencies throughout the experiment. The following section will elaborate on the possible problems within the experiment that caused these inconsistencies as well as what can be done to improve the experimental design.

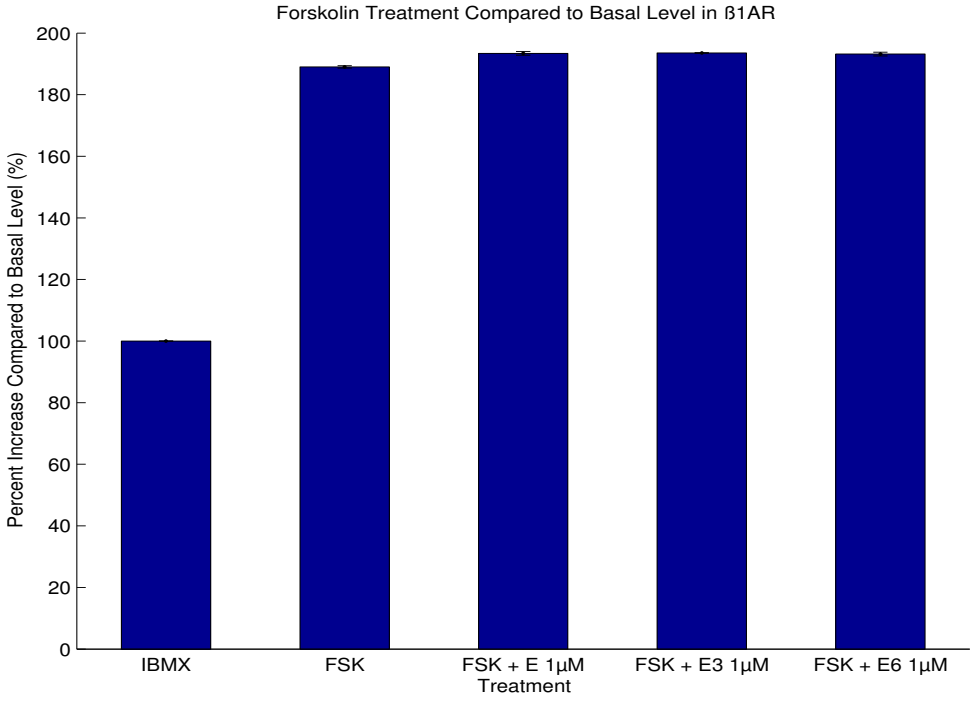

Figure 3.5: Assay 1. Plot of specific treatments versus the percent increase compared to the basal level (%). Cells were treated with Forskolin and 1μM concentrations of deuterated and non-deuterated epinephrine. HEK293 cells were transfected with β_1 adrenergic receptors. In this figure, cells treated with IBMX had an activity level set to 100%. Results indicated that treatments with Forskolin produced at least a 90% increase in cAMP production. It also showed that adding 1μM of agonist to Forskolin did not make affect the activity level greatly as Forskolin alone saturated cAMP levels.

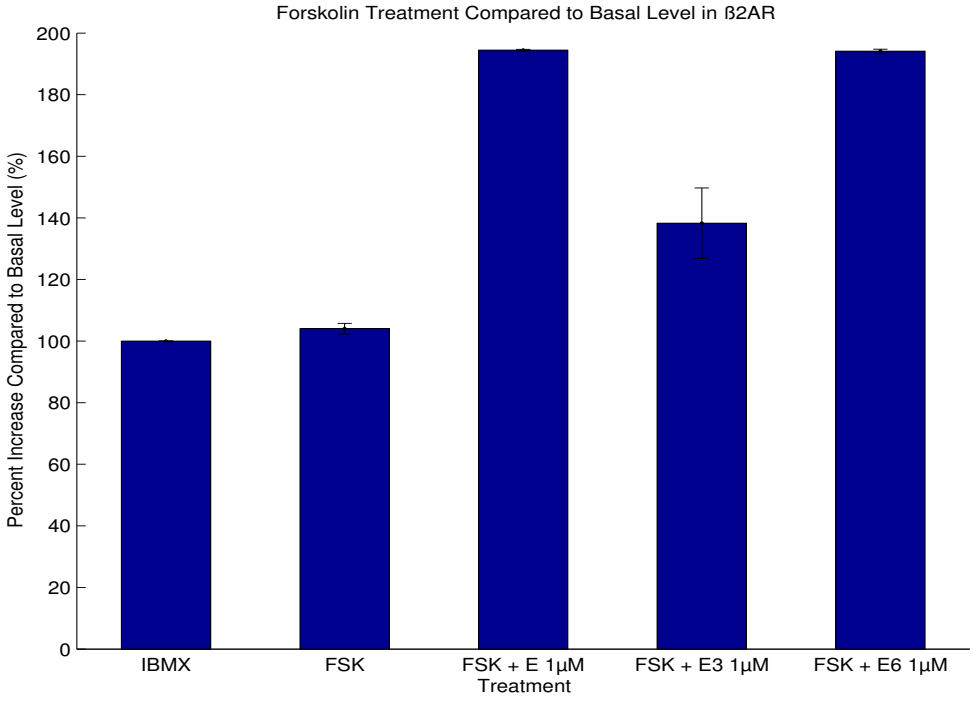

Figure 3.6: Assay 1. Plot of specific treatments versus the percent increase compared to the basal level (%). Cells were treated with Forskolin and 1μM concentrations of deuterated and non-deuterated epinephrine. HEK293 cells were transfected with β_1 adrenergic receptors at varying concentrations. In this figure, cells treated with IBMX had an activity level set to 100%. Results here were skewed and differed from Fig. 3.5. It is likely that the "FSK" and "FSK + E3 1μM" samples were lower due to human error. The other two treatments of Forskolin with epinephrine and epinephrine-d_6 indicated high levels of saturation.

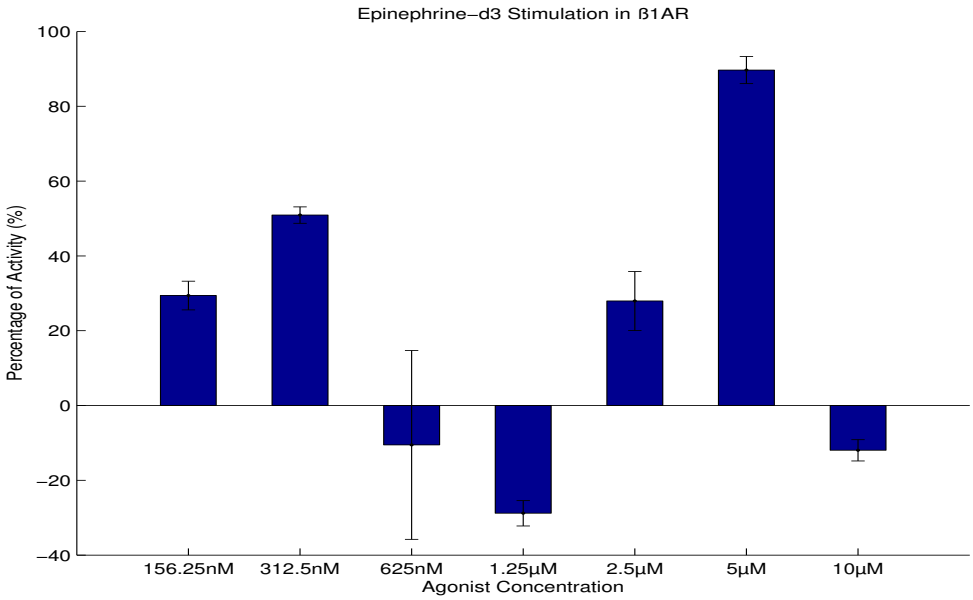

Figure 3.7: Assay 3. Plot of the agonist (epinephrine-d_3) concentration versus the percentage of activity (%). HEK293 cells were transfected with β_1 adrenergic receptors and treated with varying concentrations of agonist. Results shown here were randomly fluctuating and did not follow a clear trend.

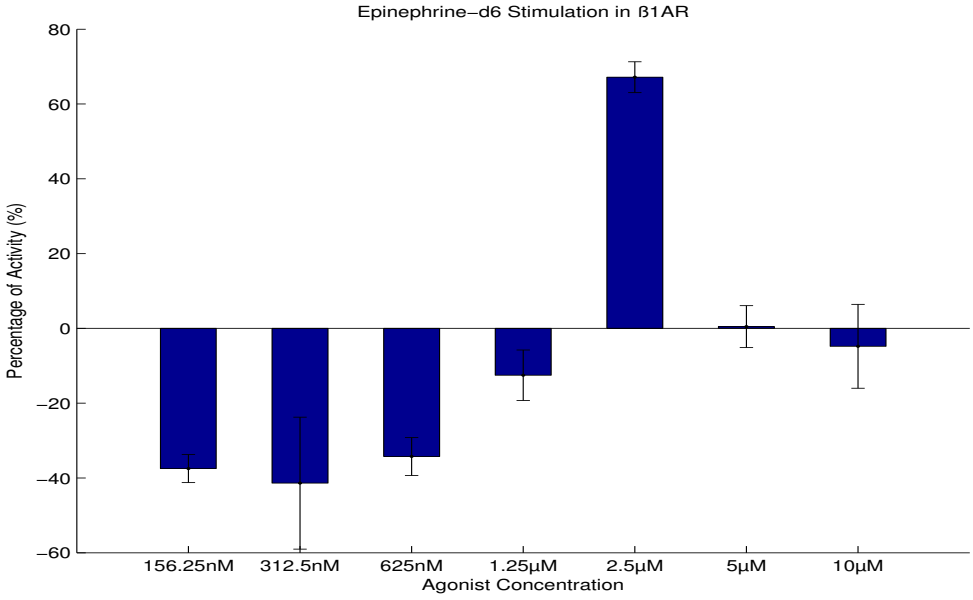

Figure 3.8: Assay 3. Plot of the agonist (epinephrine-d_6) concentration versus the percentage of activity (%). HEK293 cells were transfected with β_1 adrenergic receptors and treated with varying concentrations of agonist. Most of the results shown here were negative, implying that these samples produced less cAMP than the basal level. This plot may follow a bell curve as there seemed to be an increase in activity up to 2.5μM and then a decrease in activity after this point.

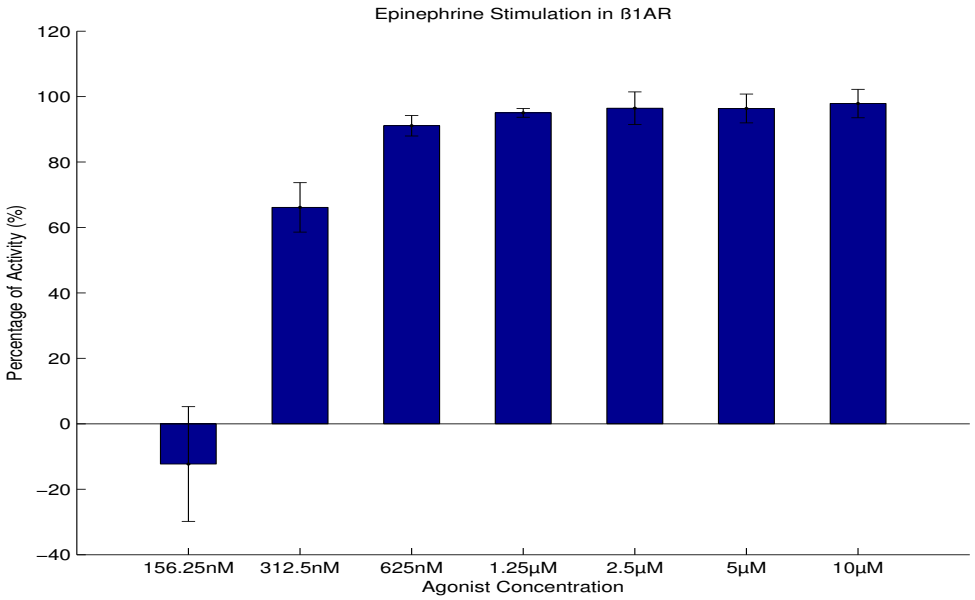

Figure 3.9: Assay 3. Plot of the agonist (epinephrine) concentration versus the percentage of activity (%). HEK293 cells were transfected with β_1 adrenergic receptors and treated with varying concentrations of agonist. Results shown here gave the typical dose-response curve of increasing activity with increasing agonist concentration. This dose-response is what is expected for the epinephrine agonist in the β-AR system.

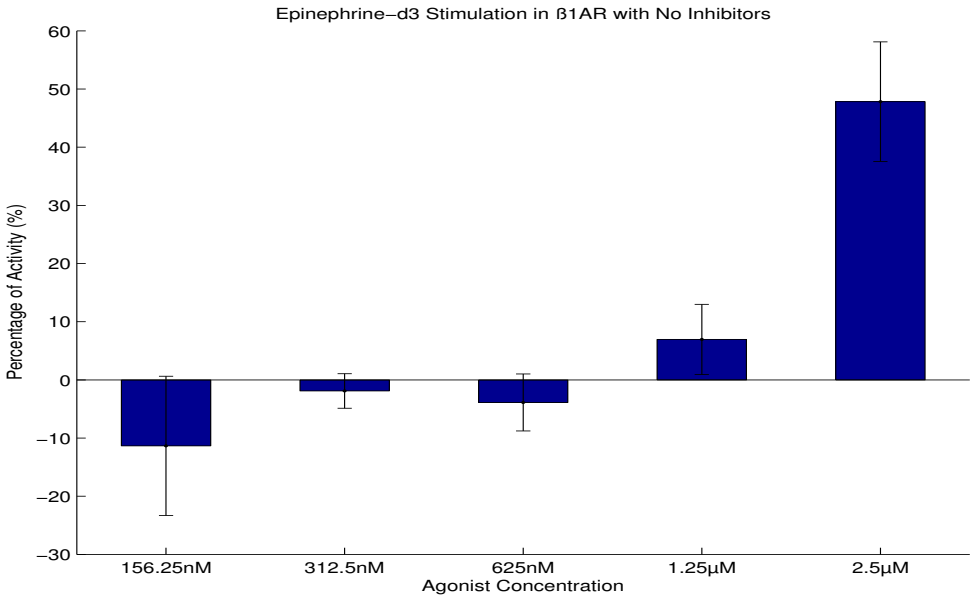

Figure 3.10: Assay 4. Plot of the agonist (epinephrine-d_3) concentration versus the percentage of activity (%). HEK293 cells were transfected with β_1 adrenergic receptors and treated with varying concentrations of agonist. The dose-response here increases with increasing agonist concentration.

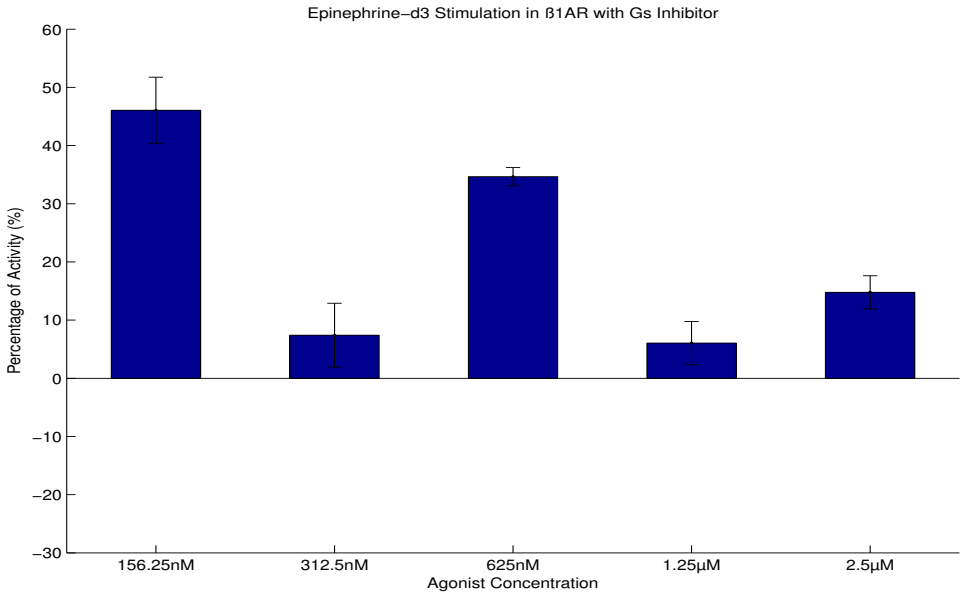

Figure 3.11: Assay 4. Plot of the agonist (epinephrine-d_3) concentration versus the percentage of activity (%). HEK293 cells were transfected with β_1 adrenergic receptors, treated with varying concentrations of agonist and G_s inhibitor. The G_s inhibitor did not seem to have worked properly for certain treatments (156.25nM and 625nM treatments) as it should have suppressed cAMP production.

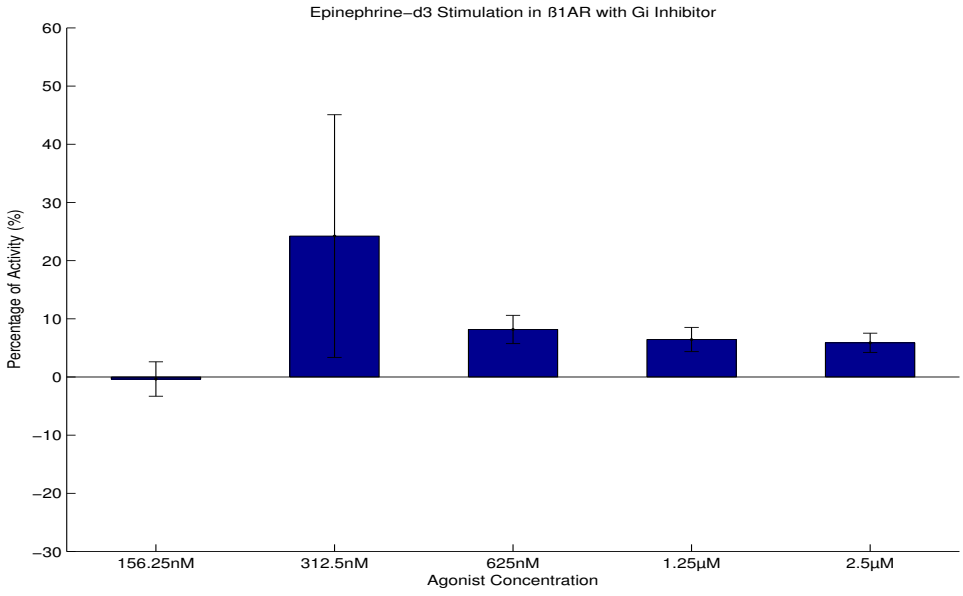

Figure 3.12: Assay 4. Plot of the agonist (epinephrine-d_3) concentration versus the percentage of activity (%). HEK293 cells were transfected with β_1 adrenergic receptors, treated with varying concentrations of agonist and G_i inhibitor. The results indicated very low levels of percentage of activity which was not expected with the addition of G_i inhibitor.

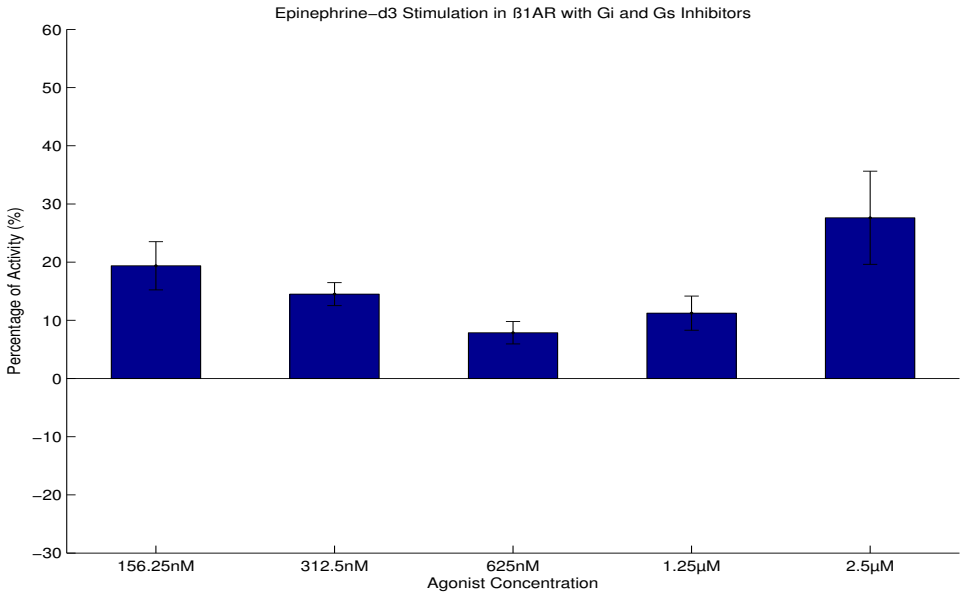

Figure 3.13: Assay 4. Plot of the agonist (epinephrine-d_3) concentration versus the percentage of activity (%). HEK293 cells were transfected with β_1 adrenergic receptors, treated with varying concentrations of agonist and G_s and G_i inhibitors. Here the activity levels are lower than 30%. Although not all of the treatments had activity levels lower than the non-inhibited values shown in Fig. 3.10, the G_s inhibitor did seem to suppress cAMP production in the 2.5μM treatment.

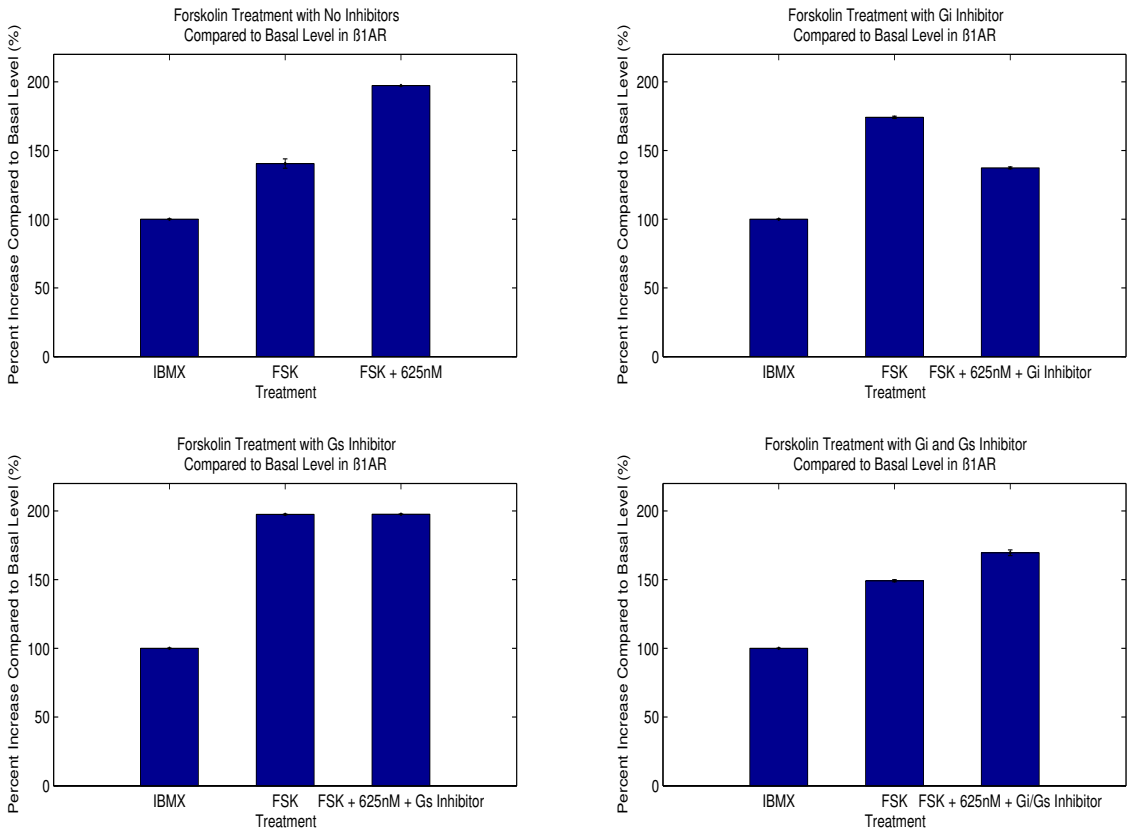

Figure 3.14: Assay 4. Plot of the agonist (epinephrine-d_3) concentration versus the percentage increase compared to the basal level (%). HEK293 cells were transfected with β_1 adrenergic receptors and treated with either Forskolin or Forskolin + 625nM of ED3 with or without an inhibitor. The percentage of activity for the sample treated with IBMX was set to 100%. The results also seemed to indicate that the G_i and G_s inhibitors did not work as planned, although Forskolin did stimulate cAMP production above the basal level.

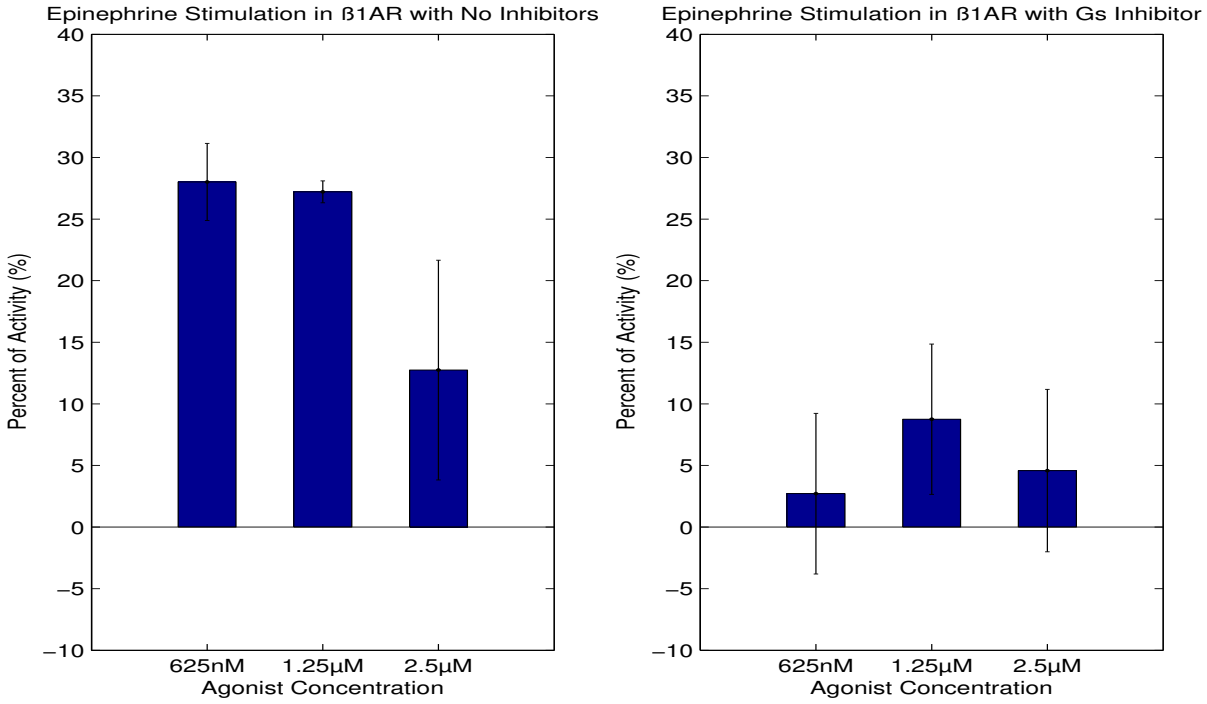

Figure 3.15: Assay 7. Plot of the agonist (epinephrine) concentration versus the percentage of activity (%). HEK293 cells were transfected with β_1 adrenergic receptors, treated with varying concentrations of agonist and G_s inhibitor. In this assay, the G_s inhibitor seemed to be effective at suppressing cAMP production.

3.3 Discussion

β_1- and β_2-adrenergic receptors are highly expressed in the heart and at varying levels of expression in the rest of the body. They are targeted by catecholamines, hormones produced by the adrenal glands, that mediate many important physiological processes. Although studies on β_2ARs primarily focus on its association with the G_s protein, various experiments have shown that this coupling is not specific. For example, β_2-ARs appear to have a biphasic effect on cardiac myocyte apoptosis (cell death), as it can cause either pro- or anti-apoptotic effects. This dual phase effect has been attributed to the receptors ability to switch coupling from G_s to G_i [33] through phosphorylation of the receptor by protein kinase A (PKA) [9]. This phenomenon has been established in reconstituted systems with recombinant proteins, cultured cells and in transgenic mice that overexpress β_2-ARs. While β_1-ARs have not been known to couple to G_i under normal circumstances, there has been evidence that it is capable of switching from G_s to G_i through a phosphorylation mechanism as well [33]. It is because of this evidence that we incorporated G_s and G_i inhibitors into our experimental procedures. Our initial results were indeterminate and no clear conclusion could be drawn as to whether or not the agonists were effective. It was hypothesized that G_s/G_i switching was occurring and was possibly affecting the amount of cAMP being produced.

The G_s/G_i switch occurs through feedback regulation. When an agonist such as epinephrine binds to a β-adrenergic receptor, G_s-mediated stimulation of adenylyl cyclase occurs and leads to an increase in the intracellular concentration of cAMP. The accumulation of cAMP activates PKA, a family of enzymes that have several important functions in the cell such as the regulation of glycogen and lipid metabolism. Both β-ARs have PKA phosphorylation sites (specific peptide sequences) located in the third intracellular loop and the carboxy-terminal tail of the receptor. Phosphorylation of these sites by PKA have been shown to decrease coupling between G_s and increase coupling to G_i for β-ARs [9, 42]. Fig. 3.16 depicts parts of the signal transduction pathways regulated by the G_s and G_i subunits that culminate in the production of extracellular signal-regulated kinase (ERK), a protein involved in regulating cell growth. The G_i subunit can activate ERK but can also inhibit adenylyl cyclase [28].

If a switch in coupling was occurring, addition of G_i inhibitors should prevent an increase in G_i-receptor coupling and prevent levels of cAMP from decreasing unexpectedly. Cells treated with G_s inhibitors should show very low levels of cAMP, while cells treated with G_i should produce levels of cAMP that increase with increasing agonist concentration until it plateaus at saturation levels. Despite the inclusion of G_s and G_i inhibitors, we did not see any clear evidence of a G_s/G_i switch occurring, as we did not consistently see the expected trends.

There have been disagreements that such a switch in G protein coupling occurs. A study performed by Friedman et al. 2002, suggests that there is a lack of evidence that

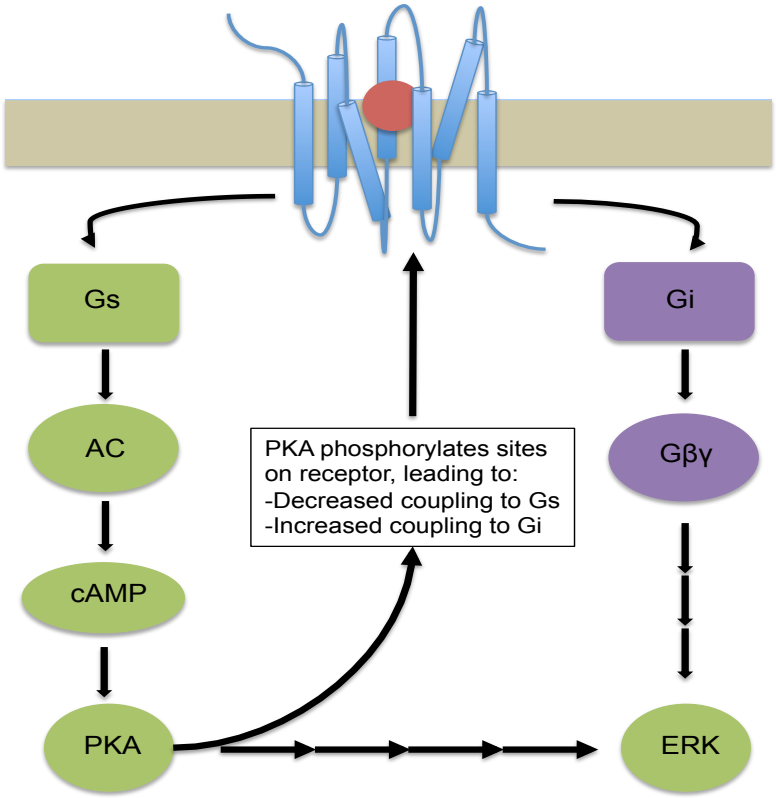

Figure 3.16: The signal transduction pathways initiated by the G_s and G_i subunits. The G_s subunit activates adenylate cyclase which stimulates the production of cAMP. Higher concentrations of cAMP in the cell activates protein kinase A (PKA), a family of enzymes capable of phosphorylating other proteins. PKA can phosphorylate the β-ARs which decreases the receptor's coupling to G_s and increase coupling to G_i. The multiple arrows in succession represent multiple steps that are not shown.

the β_2AR associates with the G_i protein. Their study, which also used the HEK293 cell line, indicated that a downstream effector, extracellular signal-regulated kinase (ERK), is activated solely through the G_s protein which disagrees with studies put forth by others that indicated the possible G_s/G_i switch [9, 42]. However, it has been argued that HEK293 cell lines do not share uniform properties as they can vary from cell line to cell line. This variability may be caused by prolonged culture where the lines may alter in chromosome number, gene expression signaling pathways and structure [28]. As to whether or not the variability in the HEK293 cells used in our experiment have affected the results is unknown. This cell line has been used before in other experiments and no major effects caused by the cell line have been noted.

Aside from a possible G_s/G_i switch, there are two other speculations as to what has caused the inconsistencies in the results. Firstly, the epinephrine compounds that were used in this experiment were dissolved in 100% DMSO. Epinephrine is soluble in hydrochloric acid (HCl) and is usually prepared in a salt form, either as epinephrine hydrochloride or as an epinephrine bitartrate salt. These compounds are easily dissolved in water and will not precipitate out of solution. However, deuterated epinephrine compounds are usually not prepared in salt form. We avoided acquiring compounds in different phases or solutions as differences in the preparation could have contributed to differences in the experiment. For this reason, all epinephrine compounds were purchased in powder form and prepared in the laboratory using 100% DMSO. DMSO was added in small increments until the epinephrine compound just dissolved. The purpose of doing this was to minimize the amount of DMSO that would eventually be added into the cell culture medium as high concentrations of DMSO can cause cell death. It is not advisable to have more than 0.5% of DMSO in the resulting medium as levels above this are cytotoxic to cells.

Despite DMSO being a universal solvent, we found that unless adequate mixing and agitation was performed, precipitates would form in the solution. It is possible that while treating the cells, the addition of the epinephrine solutions into the medium caused the epinephrine to precipitate out and reduce its effectiveness. As to how much epinephrine could have precipitated out of solution, this is unclear and could explain why the results often followed no trend. Hydrochloric acid could have been used to prepare the compounds instead of DMSO to fully dissolve the epinephrine into solution. However, doing so could have affected the pH of the cells and also promote cell death.

The second issue that could have affected the consistency of the results is the sensitivity of the kit used to quantify the amount of cAMP produced. Based on the manufacturer's data, the kit quantifies cAMP in the nanomolar range. If our samples have concentrations of cAMP lower than the nanomolar range, it would explain why the higher concentrations of epinephrine and Forskolin samples tend to generally show the high saturation levels that we expect while the lower concentrations tend to have very minimal activity percentages.

The assay kit also does not list a total protein concentration that should be loaded into

each well of the plate and only suggests that 6-100 x 10^3 cells/well be used. Overloading the plate with high concentrations of protein affects the accuracy of the results as it causes each of the wells to reach the maximum saturation levels. For our experiments, the protein amount loaded into each well was normalized to the sample with the lowest protein amount. This protein concentration varied between assays but would generally range from 40-50μg of protein per 50μL sample. Normalizing the samples beforehand ensures that all samples have the same protein concentration and that differences in the results would not be attributed to certain samples having higher cellular content. We calculated the protein concentration that would result from the manufacturer's suggested number of cells/well and this range was found to be around 10μg of protein per 50μL of sample.

As can be seen, there is still a considerable amount of trouble-shooting and problem-solving that must be done to perfect the experimental setup and to obtain consistent and accurate results. A simple experiment can be done to determine whether the compounds or the kit are affecting the current experiments. One would need an assay kit that can detect cAMP in the picomolar range and an epinephrine salt compound. The epinephrine salt and the epinephrine/DMSO solution can be used to treat the cells used previously and the same procedures and methods can be used to prepare the samples for an ELISA. Running the two compounds in parallel in an assay kit with better sensitivity should allow one to see the differences between the two epinephrine solutions and assay kits. If it is the epinephrine solubility that is affecting the outcome, then more studies will have to be done to determine how to properly prepare the epinephrine solutions. For instance, if the compounds must be dissolved in HCl, then a major issue may be determining how to alter the pH so that it does not affect cell growth and development.

Chapter 4

Conclusion

4.1 Summary

In this thesis we have discussed both theoretical and experimental work. In the theoretical section, we recognized that there is a lack of theoretical models that can accurately describe biological and chemical reactions. Our goal was to develop such a model by merging the work done by Caldeira and Leggett regarding particles coupled to phonon baths and the method developed by Auerbach and Kivelson which decomposes a complicated potential energy landscape into manageable pieces. We were also able to include both diagonal and non-diagonal couplings in our model by considering Holstein and Peierls coupling in our system. This allowed us to calculate the path integrals inside and outside a potential well for a particle coupled to a phonon bath. The path decomposition expansion formalism developed by Auerbach and Kivelson then allowed us to connect these pieces together in order to determine the full dynamics of the system.

In the experimental portion of this thesis, our goal was to determine whether enzyme-substrate binding would be affected by deuteration, or changes in molecular vibrational modes. We studied the effects of deuterated and non-deuterated epinephrine on the β-AR system. We performed a biological assay by exposing deuterated and non-deuterated epinephrine to β_1 and β_2 adrenergic receptors and then determined the amount of cAMP produced. Our aim was to determine whether deuterated compounds could significantly affect second messenger production. If a significant difference was seen, this could indicate evidence that enzyme-substrate binding may rely on more than just shape for effective binding but also on the vibrational spectra of the molecules involved. Unfortunately, our results were inconsistent and no clear conclusions could be drawn as to whether a molecular vibration-sensing mechanism occurred here.

4.2 Future Work

The theoretical model discussed in the previous chapters can be used to model various biological and chemical reactions with complicated potential energy landscapes. While we have provided the theoretical framework here, experimental or numerical work should be done to determine the validity of this model.

As for the experimental portion of this work, there are a few possible issues that need

to be considered in order for this work to continue forward. These are the possibility of G_i/G_s switching, poor sensitivity of the assay kit and epinephrine's weak solubility in DMSO. The solubility issues are most likely what caused the nonsensical nature of our results as the random precipitation of epinephrine from the solution would have affected cAMP levels. Troubleshooting and revision of the experiment must be done before we can draw conclusions about the validity of a molecular vibration-sensing mechanism in GPCR systems. If these issues can be resolved, then the results should provide a better indication of whether deuteration can affect enzyme-substrate binding in this system.

Bibliography

[1] A. Auerbach and S. Kivelson. Path decomposition for multdimensional tunneling. *Physical Review Letters*, 64(5):411, 1984.

[2] A. Auerbach and S. Kivelson. The path decomposition expansion and multidimensional tunneling. *Nuclear Physics B*, 257:799–858, 1985.

[3] J. C. Brookes, F. Hartoutsiou, A. P. Horsfield, and A. M. Stoneham. Could humans recognize odor by phonon assisted tunneling? *Physical Review Letters*, 98(3):1–10, 2007.

[4] E. Burnstein and S. Lundqvist, editors. *Tunneling Phenomena in Solids*. Plenum Press, New York, 1969.

[5] D. B. Bylund, D. C. Eikenberg, J. P. Hieble, S. Z. Langer, R. J. Lefkowitz, K. P. Minneman, P. B. Molinoff, R. R. Ruffolo, and U. Trendelenburg. of Pharmacology of Adrenoceptors. *Pharmacological reviews*, 46(2):121–136, 1994.

[6] A. O. Caldeira and A. J. Leggett. Quantum tunnelling in dissipative systems. *Annals of Physics*, 149(2):374–456, 1983.

[7] C. G. Callan and S. Coleman. Fate of the false vacuum. II. First quantum corrections. *Physical Review D*, 16(6):1762–1768, 1977.

[8] S. R. Coleman. The Fate of the False Vacuum. 1. Semiclassical Theory. *Physical Review D*, 15(4):2929–2936, 1977.

[9] Y. Daaka, L. M. Luttrell, and R. J. Lefkowitz. Switching of the coupling of the beta(2)-adrenergic receptor to different G proteins by protein kinase A. *Nature*, 390(6655):88–91, 1997.

[10] Lakshmi A. Devi, editor. *The G Protein-Coupled Receptors Handbook*. Humana Press Inc., Totowa, New Jersey, 2005.

[11] G. B. Downes and N. Gautam. The G protein subunit gene families. *Genomics*, 62(3):544–552, 1999.

[12] R. P. Feynman. *Statistical Mechanics*. W. A. Benjamin, Inc., New York, 1972.

[13] R. P . Feynman and F. L . Vernon. The theory of a general quantum system interacting with a linear dissipative system. *Annals of Physics*, 24:118–173, 1963.

[14] M. I. Franco, L. Turin, A. Mershin, and E. M. C. Skoulakis. Molecular vibration-sensing component in Drosophila melanogaster olfaction. *Proceedings of the National Academy of Sciences of the United States of America*, 108(9):3797–3802, 2011.

[15] R. Fredriksson, M. C. Lagerström, L. Lundin, and H. B. Schiöth. The G-protein-coupled receptors in the human genome form five main families. Phylogenetic analysis, paralogon groups, and fingerprints. *Molecular pharmacology*, 63(6):1256–1272, 2003.

[16] J. Friedman, B. Babu, and R. B. Clark. Beta(2)-adrenergic receptor lacking the cyclic AMP-dependent protein kinase consensus sites fully activates extracellular signal-regulated kinase 1/2 in human embryonic kidney 293 cells: lack of evidence for G(s)/G(i) switching. *Molecular pharmacology*, 62(5):1094–102, 2002.

[17] N. Fukushima, M. Kohno, T. Kato, S. Kawamoto, K. Okuda, Y. Misu, and H. Ueda. Melittin, a metabostatic peptide inhibiting G(s) activity. *Peptides*, 19(5):811–819, 1998.

[18] S. Gane, D. Georganakis, K. Maniati, M. Vamvakias, N. Ragoussis, E. M. C. Skoulakis, and L. Turin. Molecular Vibration-Sensing Component in Human Olfaction. *PLoS ONE*, 8(1), 2013.

[19] U. Gether. Uncovering molecular mechanisms involved in activation of G protein-coupled receptors. *Endocrine reviews*, 21(1):90–113, 2000.

[20] J. R. Hepler and A. G. Gilman. G proteins. *Trends in biochemical sciences*, 17(10):383–387, 1992.

[21] S. J. Hill and J. G. Baker. The ups and downs of Gs- to Gi-protein switching. *British Journal of Pharmacology*, 138(7):1188–1189, 2003.

[22] N. Holonyak, I. A. Lesk, R. N. Hall, J. J. Tiemann, and H. Ehrenreich. Direct observation of phonons during tunneling in narrow junction diodes. *Physical Review Letters*, 3(4):167–168, 1959.

[23] A. L. Hopkins and C. R. Groom. The druggable genome. *Nature reviews. Drug discovery*, 1(9):727–730, 2002.

[24] S. Jahnichen. Beta-2 Adrenergic Receptor.

[25] I. G. Lang and Y. A. Firsov. Kinetic Theory of Semiconductors with Low Mobility. *Soviet Journal of Experimental and Theoretical Physics*, 16(5):1301–1312, 1963.

[26] A. Laurenza, E. M. Sutkowski, and K. B. Seamon. Forskolin: a specific stimulator of adenylyl cyclase or a diterpene with multiple sites of action? *Trends in pharmacological sciences*, 10(November):442–447, 1989.

[27] R. J. Lefkowitz. Historical review: A brief history and personal retrospective of seven-transmembrane receptors. *Trends in Pharmacological Sciences*, 25(8):413–422, 2004.

[28] R. J. Lefkowitz, K. L. Pierce, and L. M. Luttrell. Dancing with different partners: protein kinase a phosphorylation of seven membrane-spanning receptors regulates their G protein-coupling specificity. *Molecular pharmacology*, 62(5):971–974, 2002.

[29] A. J. Leggett, S. Chakravarty, A. T. Dorsey, M.P.A. Fisher, A. Garg, and W. Zwerger. Dynamics of the Dissipative Two-State System. *Reviews of Modern Physics*, 59(1):1–85, 1987.

[30] G. Liapakis, W. C. Chan, M. Papadokostaki, and J. A. Javitch. Synergistic contributions of the functional groups of epinephrine to its affinity and efficacy at the beta2 adrenergic receptor. *Molecular pharmacology*, 65(5):1181–1190, 2004.

[31] D. J J Marchand, G. De Filippis, V. Cataudella, M. Berciu, N. Nagaosa, N. V. Prokof'Ev, a. S. Mishchenko, and P. C E Stamp. Sharp transition for single polarons in the one-dimensional su-Schrieffer-Heeger model. *Physical Review Letters*, 105(26):1–4, 2010.

[32] Dominic J. J. Marchand, P. C. E. Stamp, and M. Berciu. The polaron paradigm: a dual coupling effective band model. *arXiv preprint arXiv:1609.03096*, pages 1–20, 2016.

[33] N. P. Martin, E. J. Whalen, M. A. Zamah, K. L. Pierce, and R. J. Lefkowitz. PKA-mediated phosphorylation of the β1-adrenergic receptor promotes Gs/Gi switching. *Cellular Signalling*, 16(12):1397–1403, 2004.

[34] H. Mukai, E. Munekata, and T. Higashijima. G Protein Antagonists. *Journal of Biological Chemistry*, 267(23):16237–16243, 1992.

[35] K. B. Seamon, W. Padgett, and J. W. Daly. Forskolin: unique diterpene activator of adenylate cyclase in membranes and in intact cells. *Proceedings of the National Academy of Sciences of the United States of America*, 78(6):3363–3367, 1981.

[36] J. Shonberg, R. C. Kling, P. Gmeiner, and S. Löber. GPCR crystal structures: Medicinal chemistry in the pocket. *Bioorganic & Medicinal Chemistry*, 23(14):3880–3906, 2015.

[37] Y. Sun, J. Huang, Y. Xiang, M. Bastepe, H. Jüppner, B. K. Kobilka, J. J. Zhang, and X. Huang. Dosage-dependent switch from G protein-coupled to G protein-independent signaling by a GPCR. *The EMBO Journal*, 26(1):53–64, 2007.

[38] C. G. Tate. A crystal clear solution for determining G-protein-coupled receptor structures. *Trends in Biochemical Sciences*, 37(9):343–352, 2012.

[39] L. Turin. A Spectroscopic Mechanism for Primary Olfactory. *Chemical Senses*, 21(6):773–791, 1996.

[40] L. Turin. A method for the calculation of odor character from molecular structure. *Journal of theoretical biology*, 216(3):367–385, 2002.

[41] N. Wettschureck and S. Offermanns. Mammalian G proteins and their cell type specific functions. *Physiological Review*, 85(4):1159–1204, 2005.

[42] A. M. Zamah, M. Delahunty, L. M. Luttrell, and R. J. Lefkowitz. Protein Kinase A-mediated Phosphorylation of the beta 2-Adrenergic Receptor Regulates Its Coupling to Gs and Gi. *Journal of Biological Chemistry*, 277(34):31249–31256, 2002.